# Angle-resolved uv photoemission and electronic band structures of the lead chalcogenides

Thomas Grandke, Lothar Ley, and Manuel Cardona
*Max-Planck-Institut für Festkörperforschung, D-7000 Stuttgart 80, Federal Republic of Germany*
(Received 15 May 1978)

Angle-resolved photoemission spectra of single-crystal PbS, PbSe, and PbTe have been measured employing 16.85- and 21.22-eV excitation energies. A quite general theory of photoemission, aimed at interpreting the experimental results, is outlined. Two simple models (the direct- and nondirect-transition model) derived from this theory under rather drastic assumptions can only partially account for the experimental data. In contrast, angle-resolved photoemission spectra calculated employing the more sophisticated "weighted-indirect-transition model" agree well with the measured ones. The basic improvement inherent in this model is the consideration of the finite photoelectron lifetimes and the resulting actual relaxation of momentum conservation in the direction normal to the surface. Furthermore, the experimental results are compared in detail with the predictions of four independent band-structure calculations. Best overall agreement is found with the calculations from first principles (augmented plane wave, orthogonal plane wave).

## I. INTRODUCTION

Angle-resolved photoemission from single crystals is now widely being used for band-structure determinations.[1] The basic concept invoked is the simultaneous determination of the energy of the initial states and their locations in the Brillouin zone. However since a single-crystal surface represents a system with two-dimensional translational symmetry, only the electronic wave-vector component parallel to the surface, $\vec{k}_{\parallel}$, is conserved to within a surface reciprocal-lattice vector $\vec{g}$ during the photoemission process.[2] The corresponding wave-vector component of the initial states contributing to the angle-resolved photocurrent is trivially determined through the kinetics of the escaping photoelectrons. Strictly speaking, this only holds at zero temperature, but no important relaxation of $\vec{k}_{\parallel}$ conservation due to thermal disorder has been found at room temperature in the uv regime with perhaps one exception.[3]

On the other hand, $k_{\perp}$ is not a good quantum number because of the lack of translational symmetry in the corresponding direction and no information about it can be directly obtained from the photoemitted electrons. To circumvent this problem, two simple models have usually been employed for the assignment of $k_{\perp}$ to the initial state: (i) In the direct-transition model based on the well-known three-step process[4] (photoabsorption, transport of the photoelectron to the surface, transmission through the surface), the first step is treated as a process conserving $\vec{k}_{\parallel}$ and $k_{\perp}$, thus $k_{\perp}$ is determined through the requirement of energy and wave-vector conservation. (ii) In the nondirect model, all initial states with a given $\vec{k}_{\parallel}$ and arbitrary $k_{\perp}$ contribute to the angle-resolved photocurrent, with approximately the same weight. Consequently peaks are observed related to the singularities in the one-dimensional density of valence states along a line defined by $|\vec{k}_{\parallel}| = \text{const}$. Although the interpretation of a given spectrum in terms of a band structure may be very different for the two models, nearly no theoretical support has been given so far for either of them. In particular, it is dubious whether the complete neglect of the surface on the first step of the direct-transition model is permissible in view of the small escape depths (~5–15 Å) of uv-excited photoelectrons. Very recently, however, Pendry[5] has demonstrated that the results of his more sophisticated theory are fully consistent with the predictions of the direct-transition model in the case of Cu(001).

Clearly more experimental and theoretical work is necessary in order to exploit the full potential of angle-resolved photoemission for band-structure investigations. Such work has to employ materials with rather well-known band structures to ensure that only one crucial problem is being dealt with at a time. In this context the "lead salts" PbS, PbSe, and PbTe appear to be suitable candidates, because their electronic properties have been the subject of numerous experimental and theoretical investigations. This is partially due to interest in their fundamental properties, and partially due to their technological importance as infrared radiation emitters and detectors. All three compounds have been found to be narrow-gap semiconductors with band gaps of 0.29 eV (PbS), 0.17 eV (PbSe) and 0.19 eV (PbTe) at 4 K.[6] They crystallize in the rocksalt structure, the lattice constant $a$ is 5.929 Å, 5.117 Å, and 6.443 Å, respectively, at 300 K.[7]

The first reflectivity measurements on these materials were carried out by Cardona and Green-

 

away.[8] Since then numerous experiments investigating the electroreflectance, theremoreflectance, and wavelength-modulated reflectance in a wide range of energies have been published.[9-12] The optical properties of the lead chalcogenides have also been explored by means of electron energy-loss measurements[13,14] and by reflectivity measurements with synchrotron radiation.[15,16] Photoemission spectra of the conventional angle-integrated type have been obtained in the uv range[17,18] as well as in the x-ray range.[19]

Several computational schemes have been employed to calculate the electronic band structure of the lead salts. Herman *et al.*[20] have utilized the orthogonalized-plane-wave (OPW) method, other authors[21,22] the augmented-plane-wave (APW) method, Overhof and Rössler[23] the Korringa-Kohn-Rostoker (KKR) method, and finally a number of authors[11,24-26] have used different schemes based on the empirical-pseudopotential method (EPM). All calculated band structures exhibit a direct energy gap at the $L$ point, as may be seen in Fig. 1 for PbSe.[11] Also the overall energy-band picture is the same for the three compounds in most of the calculations. There exists, however, some quantitative disagreement with respect to the precise energies of the various bands. This especially applies to the binding energies of both the cation and anion $s$ bands (the two lowest bands in Fig. 1), but also to the relative spacings within the three $p$-derived bands (the third, fourth, and fifth valence bands). The situation is similar in the lowest conduction bands, but we shall not discuss them here because they are not accessible with photoemission spectroscopy.

Spin-orbit interaction is of particular importance in the valence bands of the lead chalcogenides besides other relativistic effects. Since the valence bands are mainly derived from atomic anion $p$ levels, spin-orbit splittings are quickly increasing along the sequence PbS-PbSe-PbTe according to the atomic number of the corresponding anion. The first direct experimental information about the magnitude of these splittings has been obtained by the present authors,[27] a more complete account of the results will be given in this publication.

In Sec. II, we start with a short description of a theory of photoemission which is similar to that of

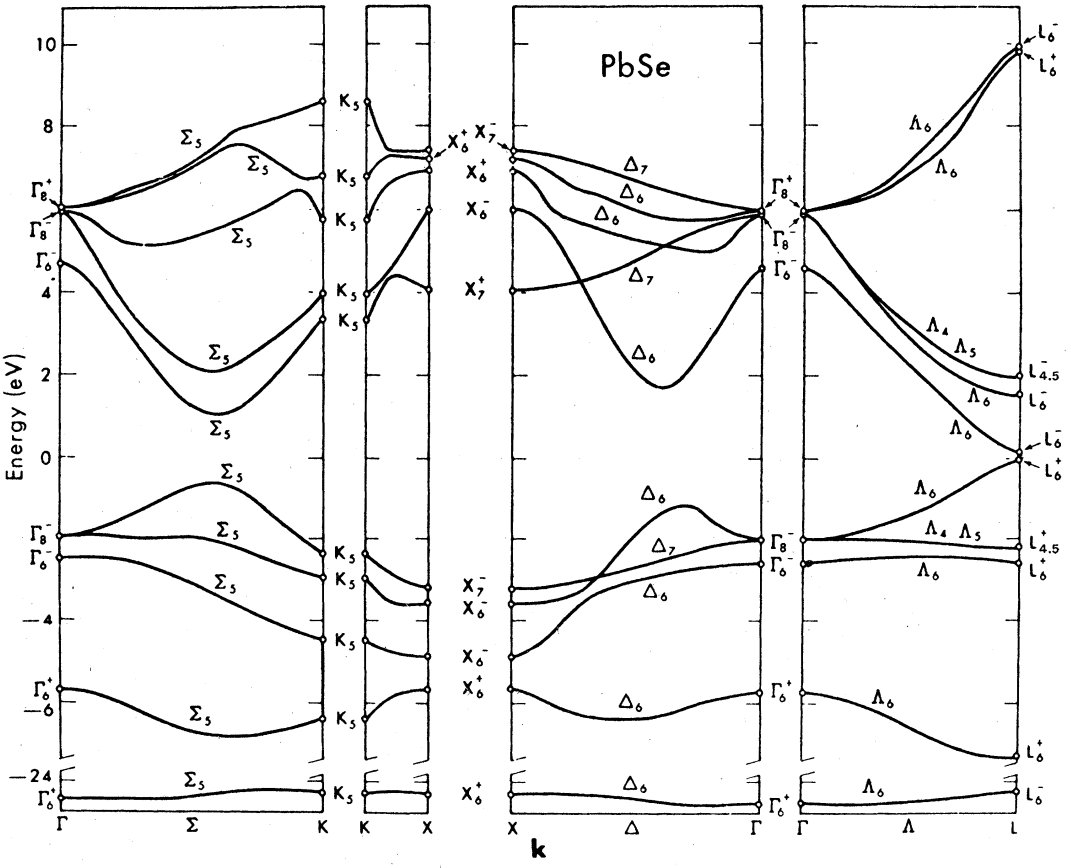


FIG. 1. EPM band structure of PbSe [after Kohn *et al.* (Ref. 11)].

Feibelman and Eastman[31] and represents the theoretical background of this work. We shall demonstrate that the two simple models mentioned above are contained as limiting cases in this more general theory and review the utilization of these models in interpreting angle-resolved photoemission measurements. In Sec. III, we describe the experimental procedures, while in Sec. IV, the results are first discussed in the light of different approximations of the full theory of photoemission outlined in Sec. II. A comprehensive comparison between calculated and experimental critical point energies with special emphasis on the spin-orbit splittings is also provided in Sec. V.

## II. THEORY OF PHOTOEMISSION

### A. General expression for the differential photocurrent

Several authors[28-31] have shown that the process of photoemission from a solid may be treated by using a Golden Rule formula (in atomic units with $\hbar = m = e = 1$):

$$j(\vec{R},E) \sim \frac{\sqrt{E}}{R^2} \sum_j \delta(E-\omega-E_j) \times \left| \int d^3r\, \phi^*(\vec{r},\vec{R},E) O(\vec{r}) \psi_j(\vec{r}) \right|^2 . \tag{1}$$

The sum extends over all occupied states $\psi_j$, while $\phi$ represents a time-reversed LEED state, which is identical to the final state encountered in photoemission.[28,29,31] $\vec{R}$ is a vector pointing from the surface towards the detector, and $\omega$ is the photon energy. The operator $O(\vec{r})$ represents the interaction between photon and electron. Neglecting local-field corrections and the spatial variation of the vector potential, we replace $O(\vec{r})$ by the constant amplitude $a_{sc}$ of the screened vector potential and the polarization vector $\vec{e}$,

$$O(\vec{r}) = -i a_{sc} \vec{e} \cdot \nabla . \tag{2}$$

In order to derive a more suitable expression for the differential photocurrent, we closely follow the treatment by Feibelman and Eastman.[31] Their Eq. (49) is, however, based on the neglect of the inelastic damping effects which give rise to the possibility of indirect transitions. In what follows, we shall derive a more general expression which includes this possibility. We assume that the surface is unreconstructed. The initial- and final-state wave functions may then be written as two-dimensional Bloch functions of the surface coordinate $\vec{\rho} = (x,y)$:

$$\phi(\vec{r},\vec{R},E) = \exp(i\vec{k}_{\parallel}^{r} \cdot \vec{\rho}) U(\vec{\rho},z;\vec{R},E) , \tag{3a}$$

$$\psi_j(\vec{r}) = \psi^{(n)}_{\vec{p}_{\parallel},p_{\perp n}}(\vec{r}) = \exp(i\vec{p}_{\parallel} \cdot \vec{\rho})\, V^{(n)}_{\vec{p}_{\parallel},p_{\perp n}}(\vec{\rho},z) . \tag{3b}$$

$U$ and $V^{(n)}$ are periodic functions of $\vec{\rho}$; $\vec{k}_{\parallel}^{r}$ is obtained from the wave-vector component parallel to the surface $\vec{k}_{\parallel}$ of the asymptotic free electrons at the point of observation by translating it back into the first Brillouin zone, while $\vec{k}_{\parallel}$ is given by the familiar relation

$$|\vec{k}_{\parallel}| = \sqrt{2E}\sin\theta . \tag{4}$$

$\theta$ is the exit angle of the photoelectrons, referred to the surface normal. The implicit index $j$ of the occupied states has been replaced by their wave vector $(\vec{p}_{\parallel},p_{\perp n})$ and their band index $n$.

Inserting the Eqs. (3a) and (3b) into the matrix element of Eq. (1) gives ($\Omega_2$ is the area of the surface unit cell)

$$j(\vec{R},E) \sim \frac{\sqrt{E}}{R^2} \sum_{n,p_{\perp n}} \delta(E-\omega-E^{(n)}_{\vec{k}_{\parallel}^{r},p_{\perp n}}) \times |M(p_{\perp n},n,\vec{R},E)|^2 , \tag{5a}$$

with

$$M(p_{\perp n},n,\vec{R},E) = \int_{\Omega_2} d^2\rho \int dz\, U^*(\vec{\rho},z,\vec{R},E) \times (\vec{e}_{\parallel} \cdot \vec{k}_{\parallel} - i\vec{e} \cdot \nabla) V^{(n)}_{\vec{p}_{\parallel},p_{\perp n}}(\vec{\rho},z). \tag{5b}$$

As direct consequence of the two-dimensional translational symmetry of an ideal crystal surface, only those valence states with $\vec{p}_{\parallel} = \vec{k}_{\parallel}^{r} = \vec{k}_{\parallel} + \vec{g}$ contribute to the angle-resolved photocurrent. For the calculation of the two-dimensional periodic functions $U$ and $V^{(n)}$ let us assume that the one-electron potential is the ideal crystal potential with three-dimensional periodicity for $z \geq 0$, separated from the vacuum region by a smooth barrier with center at $z = 0$. Then $U$ inside the crystal may be expressed as a linear combination of Bloch functions of the coordinate $z$,

$$U(\vec{\rho},z,R,E) = \sum_{n''} T_{n''}(\vec{k}_{\parallel},E) \exp[ik_{\perp n''}(\vec{k}_{\parallel}^{r},E)z] \times f_{n''}(\vec{\rho},z,\vec{k}_{\parallel}^{r},E). \tag{6}$$

The functions $f_{n''}$ exhibit the same periodic properties as the crystal potential. Each Bloch function is characterized by its energy $E$ and its wave vector $\vec{k} = (\vec{k}_{\parallel}, k_{\perp n''})$ where because of the presence of the surface we have to allow for the possibility of $k_{\perp}$ being complex. Thus, the first step to evaluate Eq. (6) is to compute the complex band struc-

ture, i.e., $k_{\perp r}+ik_{\perp i}$ as a function of $E$ and $\vec{k}_{\parallel}$. This could be done, in principle, with the pseudopotential method. However, because of uncertainties involving the nonlocality of the pseudopotential over wide energy ranges a "first principles" method such as KKR is usually preferred. The layer KKR method[32] automatically incorporates the two-dimensional symmetry at the surface and is thus particularly adequate for matching to plane waves in free space. Such matching is required to determine the expansion coefficients $T_{n''}(\vec{k}_{\parallel},E)$ of Eq. (6) which represent the amplitudes of Bloch waves which couple to the outgoing plane wave. We note that the Bloch states $f_{n''}\exp(ik_{\perp n''}z)$, as bulk quantities, only depend on the reduced wave-vector component $\vec{k}_{\parallel}^{\,r}$. On the other hand, the coefficients $T_{n''}(\vec{k}_{\parallel},E)$ represent the coupling between a region of translational symmetry (the periodic crystal) and a region of translational invariance (the vacuum). Consequently, they depend on the extended wave-vector component $\vec{k}_{\parallel}$.

We emphasize that in a realistic calculation the crystal potential should have an absorptive (i.e. imaginary) part representing inelastic electron-electron interaction resulting in a finite lifetime of the photoelectrons. Consequently, *all* the $k_{\perp n''}$ will be complex, half of them with a positive imaginary part.[32] Those with negative Im $(k_{\perp n''})$ have to be discarded, because they grow exponentially into the crystal thus not showing the same limiting behavior for $z\to\infty$ as the (time reversed) LEED function $\phi(\vec{r},\vec{R},E)$. Consequently, the summation over $n''$ in Eq. (6) only extends over those Bloch waves with positive Im$(k_{\perp n''})$. Since the initial states $\psi_j$ obey different boundary conditions than the LEED function, the expansion of the functions $V^{(n)}$ into Bloch functions of the coordinate $z$ has to be written in the following form

$$V^{(n)}_{\vec{k}_{\parallel}^{\,r},\,p_{\perp n}}(\vec{\rho},z)=\exp[ip_{\perp n}(\vec{k}_{\parallel}^{\,r},E-\omega)z]\,g_n^-(\vec{\rho},z,\vec{k}_{\parallel}^{\,r},E-\omega)+\sum_{n'}C_{nn'}(\vec{k}_{\parallel}^{\,r},E-\omega)\exp[ip_{\perp n'}(\vec{k}_{\parallel}^{\,r},E-\omega)z]\,g_{n'}^+(\vec{\rho},z,\vec{k}_{\parallel}^{\,r},E-\omega)\,. \tag{7}$$

Here $p_{\perp n}$ is the normal wave-vector component of a Bloch wave with negative group velocity (i.e., running towards the surface), the possible $p_{\perp n}$ may be calculated using the layer KKR method. To ensure smoothness of the wave functions at the surface, this Bloch wave has to be matched smoothly to all Bloch waves designated by $p_{\perp n'}$, which have either a positive group velocity or a purely imaginary $p_{\perp n'}$ ("evanescent waves"). The reflection coefficients thus obtained are called $C_{nn'}(\vec{k}_{\parallel}^{\,r},E-\omega)$. In case that no Bloch wave with a real wave-vector component $p_{\perp n'}$ exists for given $\vec{k}_{\parallel}^{\,r}$ and $E-\omega$, we obtain a band gap. Surface states that may exist in such a band gap have to be represented by an expression slightly different from Eq. (7), but we will neglect them in the following. The functions $g_n^{\pm}(\vec{\rho},z,\vec{k}_{\parallel}^{\,r},E-\omega)$ exhibit the same three-dimensional periodicity as the crystal potential.

We note that neither the initial states nor the final state are eigenfunctions of the wave-vector component directed normal to the surface: The Eqs. (6) and (7) contain summations over states with different $k_{\perp n''}$ and $p_{\perp n}$, $p_{\perp n'}$, respectively. Inserting these equations into Eq. (5b) yields for the matrix element:

$$M(p_{\perp n},n,\vec{R},E)=\sum_{n''}T_{n''}\Big(\int_{\Omega_2}d^2\vec{\rho}\int_0^{\infty}dz\,\exp(-ik^*_{\perp n''}z)f^*_{n''}(\vec{e}_{\parallel}\circ\vec{k}_{\parallel}^{\,r}-i\vec{e}\cdot\nabla)\exp(ip_{\perp n}z)g_n^-
+\sum_{n'}C_{nn'}\int_{\Omega_2}d^2\vec{\rho}\int_0^{\infty}dz\,\exp(-ik^*_{\perp n''}z)f^*_{n''}(\vec{e}_{\parallel}\cdot\vec{k}_{\parallel}^{\,r}-i\vec{e}\cdot\nabla)\exp(ip_{\perp n'}z)g_{n'}^+\Big)\,. \tag{8}$$

The contribution to the integral from the interval $[-\infty,0]$ has been neglected, since the valence-band wave functions decrease very rapidly beyond the surface barrier. We now reduce the integration between $z=0$ and $z=\infty$ to an equivalent integration between $z=0$ and $z=c_{\perp}$, where $c_{\perp}$ is the spacing between equivalent layers of the ideal crystal in the direction normal to the surface. Finally we replace the summation over $p_{\perp n}$ in Eq. (5a) by an integration over $E^{(n)}_{\vec{k}_{\parallel}^{\,r},\,p_{\perp n}}$ by introducing the one-dimensional density of states along $p_{\perp n}$. The resulting expression for the angle resolved photocurrent is given by

$$j(\vec{R},E)\sim\frac{\sqrt{E}}{R^2}\sum_n\left|\frac{dE^{(n)}_{\vec{k}_{\parallel}^{\,r},\,p_{\perp n}}}{dp_{\perp n}}\right|^{-1}_{E^{(n)}_{\vec{k}_{\parallel}^{\,r},\,p_{\perp n}}=E-\omega}\left|T_{n''}(\vec{k}_{\parallel},E)\Big(\frac{1}{1-\exp[i(p_{\perp n}-k^*_{\perp n''})c_{\perp}]}\,\bar{M}^-_{n''n}+\sum_{n'}C_{nn'}(\vec{k}_{\parallel}^{\,r},E-\omega)\frac{1}{1-\exp[i(p_{\perp n'}-k^*_{\perp n''})c_{\perp}]}\bar{M}^+_{n''n'}\Big)\right|^2, \tag{9a}$$

with

$$\bar{M}^{\pm}_{n''n}=\int_{\Omega_2} d^2\vec{\rho}\int_0^{c_\perp} dz\,\exp(-ik^*_{\perp n''}z)f^*_{n''}(\vec{e}_\parallel\cdot\vec{k}_\parallel-i\vec{e}\cdot\nabla)\exp(ip_{\perp n}z)g^{\pm}_n\ . \tag{9b}$$

The reduced matrix elements represent the contribution of one unit cell of the three-dimensional crystal to the differential photocurrent. The interference between different unit cells contained in the same layer (oriented parallel to the surface) gives rise to the $\vec{k}_\parallel$ conservation, cf. Eq. (5). The interference between different layers is accounted for by the factors $\{1-\exp[i(p_{\perp n}-k^*_{\perp n''})c_\perp]\}^{-1}$, which thus represent the remnant of the conservation of crystal momentum in the $z$ direction. Only if an infinite number of layers contributes to the photocurrent (i.e., in the unrealistic case of vanishing damping), these factors reduce to the form $\delta(p_{\perp n}-k_{\perp n''})$. In the more realistic case, all $k_{\perp n''}$ are complex. Hence for a given final state $k_{\perp n''}(E,\vec{k}_\parallel)$ all those initial states $p_{\perp n}(E-\omega,\vec{k}_\parallel)$ contribute markedly to the angle-resolved photocurrent that satisfy the following condition:

$$\mathrm{Re}(k_{\perp n''})-\mathrm{Im}(k_{\perp n''})<p_{\perp n}<\mathrm{Re}(k_{\perp n''})+\mathrm{Im}(k_{\perp n''})\ . \tag{10}$$

This relaxed conservation rule may be visualized as a momentum broadening that affects the conduction bands only, cf. Fig. 2. If we neglect the interaction between the photoelectron and the hole created in the valence bands, the crystal potential is Hermitian at the energies of the occupied states and the valence bands suffer no momentum broadening.

### B. Direct transitions versus one-dimensional density of states in recent experimental work

First we discuss the origin of peaks in angle-resolved photoemission spectra on the basis of the complete expression (9) for the differential photocurrent. We note that the reduced matrix elements $\bar{M}^{\pm}_{n''n}$, the transmission coefficients $T_{n''}(\vec{k}_\parallel,E)$, and the reflection coefficients $C_{nn'}(\vec{k}_\parallel,E-\omega)$ are not likely to exhibit the strong energy dependence which is necessary to give rise to peaks with widths of less than 0.5 eV. Thus, only two factors entering Eq. (9) may depend strongly on the energy $E$, these are (i) the one-dimensional density of valence states, and (ii) the remnants of momentum conservation in the direction normal to the surface.

Consequently, the sharp structures observed in angle-resolved photoemission spectra should be due to either (a) peaks in the one-dimensional density of valence states along $p_\perp$, or (b) the fulfillment of wave-vector conservation in the direction normal to the surface, i.e., direct transitions. These two effects may readily be distinguished experimentally if different photon energies are available: Peaks that are due to the effect (a) appear at the same binding energy $E_B=E-\omega$, no matter which photon energy is employed. On the other hand, peaks arising from the effect (b) should move systematically with the photon energy, provided that we exclude the special case of valence bands which are flat along $k_\perp$ ("two-dimensional" systems). Angular resolved photoemission experiments have shown that both effects may give rise to structure in the observed spectra.

For example, a number of measurements on different surfaces of gold,[33,34] silver,[35] copper,[34,36-39] nickel,[40,41] and tungsten[42,43] could be interpreted by invoking direct (i.e., $k_\perp$ conserving) transitions between occupied and empty bulk energy bands along lines of fixed $\vec{k}_\parallel$ in reciprocal space. Particularly convincing are recent experiments on tungsten by Lapeyre *et al.*[43] and on copper by Stöhr *et al.*[39] utilizing synchrotron radiation as a continuously tunable light source. Their spectra exhibit peaks moving systematically with the photon energy $\omega$. This effect provides direct evidence for the conservation of the wave-vector component $k_\perp$. There exists, however, some controversy on the character of the conduction bands. While Lapeyre *et al.*[43] use the calculated bulk band structure[44] for the interpretation of their spectra, Stöhr *et al.*[39] approximate the conduction bands by a single plane

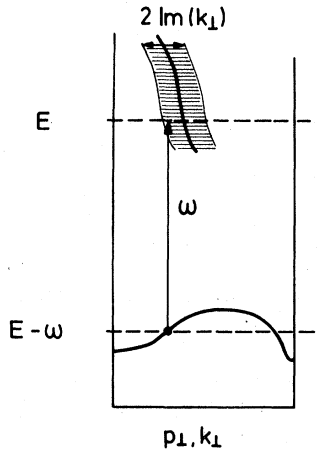


FIG. 2. Example of an indirect transition made possible on account of the momentum broadening of a conduction band.

wave. Only in the latter case a simple relation exists between $k_\perp$ in the crystal and $k_\perp^0$ in vacuum (we assume normal emission, i.e., $\vec{k}_\parallel = \vec{0}$)

$$\tfrac{1}{2}k_\perp^0 = \tfrac{1}{2}k_\perp^2 - V_0 . \tag{11}$$

$V_0$ is the height of the potential step at the surface. No inelastic damping effects were taken into account in either case.

On the other hand, the direct transition model failed to explain the experimental data obtained from the (110) surfaces of the three noble metals, copper, silver, and gold[45] and the (0001) surface of bismuth.[46] In these cases the measured spectra resembled the one-dimensional density of valence states along $k_\perp$. This result could be interpreted in terms of a complete relaxation of any $k_\perp$ conservation. On the other hand, Stöhr *et al.*[39] claim that their results obtained on Cu(110) do *not* contradict the direct transition model. Finally, Feuerbacher and Christensen[47] had to use both models simultaneously in order to explain the experimental results obtained on different surfaces of tungsten.

Thus, angle-resolved photoemission work has shown that both direct transitions and one-dimensional density of occupied states can give rise to structure in the observed spectra. It has, however, been impossible to date to predict whether one effect or the other would be predominant in a specific case. Only very recently, calculations have shown that direct transitions are the origin of all peaks in the angle-resolved photoemission spectra from the Cu(100),[5,48] and Mo(100),[48] surfaces despite a considerable relaxation of the $k_\perp$ conservation.

We have extensively used the one-dimensional density of states approach to interpret the spectra obtained from the (100) surface of PbS.[49] A brief account of these efforts will be given in Sec. IV A. A more complete understanding of angle-resolved photoemission from the lead salts must, however, be based on the full theory outlined above that does not contain any *a priori* assumptions with respect to the relative importance of features due to $k_\perp$-conserving transitions and maxima in the one dimensional density of occupied states. Such an attempt will be presented in Sec. IV B.

## III. PHOTOEMISSION MEASUREMENTS

### A. Experimental

Experiments were performed in a commercially available angle-resolving photoemission spectrometer (VG model ADES 400) in which the electron energy analyzer can be rotated about the sample. An independent rotation of the sample around the same axis gives an almost complete freedom in the choice of the incidence angle $\theta_\omega$ of the exciting photon beam and the electron acceptance angle $\theta$, all angles being referred to the surface normal of the sample. The only restriction is a coplanar arrangement of the photon beam, the electron acceptance direction and the surface normal. Physical interference between the fixed lamp and the rotating analyzer limits the angle between the photon beam and the electron acceptance direction, $|\theta - \theta_\omega|$, to values larger than ~15°. A second rotation of the sample around the surface normal allows an independent choice of its azimuthal orientation with respect to the electron acceptance direction. A system to observe low-energy electron diffraction (LEED), which is incorporated in the same ultra high-vacuum chamber, facilitates the proper selection of the azimuthal angle for the angle-resolved photoemission measurements.

The photoemission spectra of the valence band were taken using Ne I ($\hbar\omega = 16.85$ eV) or He I ($\hbar\omega = 21.22$ eV) photons delivered by a differentially pumped resonance lamp, while He II ($\hbar\omega = 40.81$ eV) photons were used for exciting electrons from the Pb $5d$ core levels. The hemispherical electrostatic electron energy analyzer was operated at a pass energy of 10 eV corresponding to a resolution of 0.3 eV. Thus, the doublet structure of the NeI radiation (satellite at $\hbar\omega = 16.67$ eV, corresponding to a splitting of 0.18 eV) could be neglected to a good approximation. The angular resolution, which is determined by the opening angle of the acceptance cone of the hemispherical analyzer, is 3°. The resulting momentum resolution, calculated from

$$\Delta|\vec{k}_\parallel| = \sqrt{2E}\,|\cos\theta|\,\Delta\theta, \tag{12}$$

is of the order of 0.02 $\text{Å}^{-1}$. Comparing this with the typical diameter of the Brillouin zone of the lead salts (2 $\text{Å}^{-1}$), one finds that only photoelectrons emerging from ~ 0.01% of the volume of the whole Brillouin zone can reach the detector on account of $\vec{k}_\parallel$ conservation during the photoemission process.

High-quality single crystals, grown by vacuum sublimation,[50] of $n$-PbSe, $p$-PbSe, and $p$-PbTe were used for the photoemission measurements, while natural single crystals were employed in the case of $n$-PbS and $p$-PbS. All samples were cleaved in vacuum along a (100) plane, the base pressure being less than $1\times10^{-10}$ Torr. Immediate *in situ* analysis of the freshly cleaved surfaces insured a surface periodicity in agreement with the two-dimensional projection of the bulk unit cell. The photoemission measurements were limited to surfaces with the sharpest possible diffraction patterns in order to minimize possible violations of the $\vec{k}_\parallel$ conservation induced by surface irregularities. A relaxation of the surface

atoms without an accompanying change of the surface periodicity may not be deduced from an analysis of the LEED pattern, since it does not affect the $\vec{k}_{\parallel}$ conservation. Serious relaxation effects are, however, only likely to occur in crystals with strong directional bonds, e.g., Si or GaAs.

The observed square diffraction patterns maintained their sharpness at least for several days. Moreover, no changes in the angular-resolved photoemission spectra could be detected during this time. Possible effects of oxygen absorption were extensively studied in the case of PbSe. But even an exposure to $10^3$ Langmuir of $O_2$ did not affect the spectra in a noticeable manner. Similar results have been reported by Hagström,[51] who found sticking coefficients of $4\times10^{-11}$ and $4\times10^{-9}$ for the absorption of oxygen on PbSe(100) and PbTe(100), respectively. Green and Lee[52] have determined a sticking coefficient of $1.3\times10^{-9}$ in the case of PbTe(100). These results confirm that the (100) surfaces of the lead salts are rather inert and that no contaminants influenced our photoemission measurements. On the other hand, a proper explanation for the extremely small sticking coefficients has yet to be found.

All photoemission spectra were recorded with a multichannel analyzer operating in the multichannel scaling mode. The energy scale was digitized in steps of 0.075 eV. Since the energy resolution of the electron analyzer was 0.3 eV, this digitizing procedure did not spoil the resolution. Reliable positions of peaks and shoulders in a spectrum were determined from its second derivative, obtained with a numerical differentiation procedure. The binding energies thus obtained have been referenced to the Fermi level. The deviation between this energy reference and the top of the valence band, which usually serves as the reference for binding energies in semiconductors, is smaller than the width of the forbidden band ($\lesssim 0.3$ eV in the lead salts), except in strongly degenerate samples. The position of the Fermi energy was determined by measuring the spectrum of the steel sample holder, previously cleaned by $\frac{1}{2}$ h of $Ar^+$-ion bombardment. The Fermi level of the sample holder should be practically identical with the Fermi level of the sample in the case of the highly conductive lead salts under consideration.

Peak intensities, which were measured as a function of the photon incidence angle $\theta_\omega$, were normalized to the maximum intensity of the tail of inelastically scattered electrons. Since the latter is not expected to vary intrinsically as a function of $\theta_\omega$ for a given light intensity, this normalization should eliminate the following two instrumental effects: (i) The illuminated area of the sample depends on $\theta_\omega$, and (ii) the intensity of the uv lamp exhibits long-time fluctuations.

### B. Results

Angle-resolved photoemission spectra were taken for two different azimuthal orientations of the single-crystal surfaces. Designating the surface normal as the [100] direction, the electron acceptance cone was chosen to lie either in the (010) plane or in the $(0\bar{1}1)$ plane. Consequently, the projection $\vec{k}_{\parallel}$ of the electron wave-vector component onto the surface was parallel to the [001] direction or to the [011] direction, respectively. These are the two high-symmetry directions present in the surface Brillouin zone of the (100) surface of a fcc crystal. The two corresponding crystal orientations differ by an azimuthal rotation of 45° about the surface normal.

In Fig. 3, we present some selected He I-in-

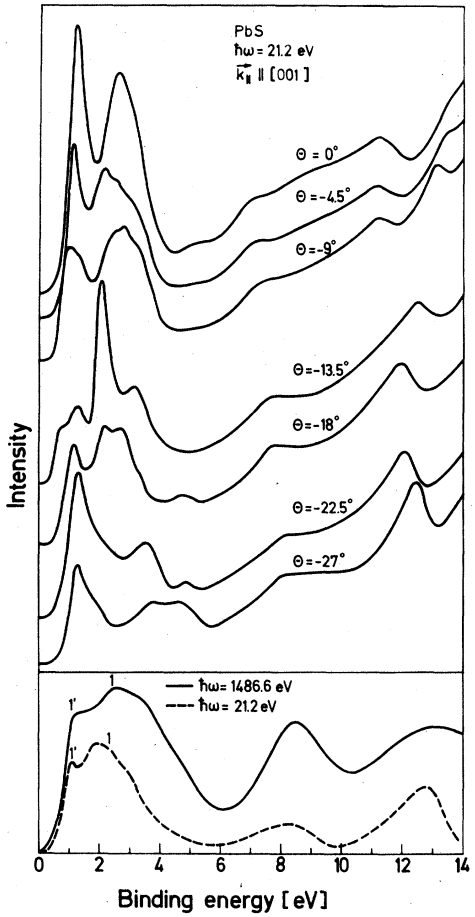


FIG. 3. Angle-resolved uv photoemission spectra, angle-integrated x-ray photoemission spectrum (Ref. 19), and uv photoemission spectrum (of polycrystalline PbS, Ref. 18). The zero of energies is taken to coincide with the Fermi level.

duced angle-resolved photoemission spectra of PbS for $\vec{k}_{\parallel} \parallel [001]$ and various electron exit angles $\theta$. All spectra shown in this figure have been taken for $\theta_\omega = 45°$, while different light incidence angles have also been used in the course of further measurements. For comparison, an angle-integrated x-ray-photoemission (XPS) spectrum[19] and a rather similar uv-photoemission (UPS) spectrum[18] of polycrystalline PbS are incorporated in the same figure. The most prominent group of peaks in the angle-resolved uv spectra appears within the first 6-eV binding energy, and it corresponds to the peaks 1 and 1′ in the XPS and UPS spectra. These peaks originate from the three $p$-type valence bands of PbS, which are mainly derived from S ($3p$) levels. Due to their comparatively low cross section for uv photoexcitation, the $s$-type bands derived from Pb $6s$ (8-eV binding energy) and S $3s$ (13-eV binding energy) levels appear only as weak structures in the angle-resolved photoemission spectra. Since secondary-electron emission (SEE) in conjunction with final-state effects is also expected to produce sharp peaks in the energy range close to the vacuum zero,[53] we shall limit the following discussion to the first 6-eV binding energy.

As has been pointed out already, the Fermi level served as reference for the energy distribution curves. The position of the Fermi level at the surface of PbS was investigated by measuring the binding energy of the Pb $5d_{5/2}$ core levels using an excitation energy of 40.81 eV (He II). The binding energy was determined to be $19.0 \pm 0.1$ eV for both $n$-type and $p$-type PbS. Thus, the Fermi level seems to be pinned by surface states at the (100) surfaces for $n$-PbS and $p$-PbS. The same result has been obtained on $n$-PbSe and $p$-PbSe. Furthermore, the binding energy did not change upon changing from normal to the more surface sensitive glancing emission. Thus, the band bending at the surface is too small to be observed within the maximum escape depth ($\lesssim 10$ Å) of the photoelectrons. This result is consistent with an estimated barrier penetration depth of 2500 Å in the highly polarizable lead salts.

In Figs. 4–6 we present the experimental peak positions $E$ versus the corresponding wave-vector component $\vec{k}_{\parallel}$ as obtained from Eq. (4) for all three lead salts. The crosses represent well-defined peaks while open symbols represent weak peaks or shoulders which have been taken from the second derivative of an original spectrum. Peak positions measured for positive ($\times, \Delta$) and negative ($+, \square$) $\vec{k}_{\parallel}$ have been superimposed. These two sets of data coincide almost perfectly, showing that the $E$-vs-$\vec{k}_{\parallel}$ plots exhibit mirror symmetry about the zone center at $\vec{k}_{\parallel} = \vec{0}$ as is being required from symmetry considerations.

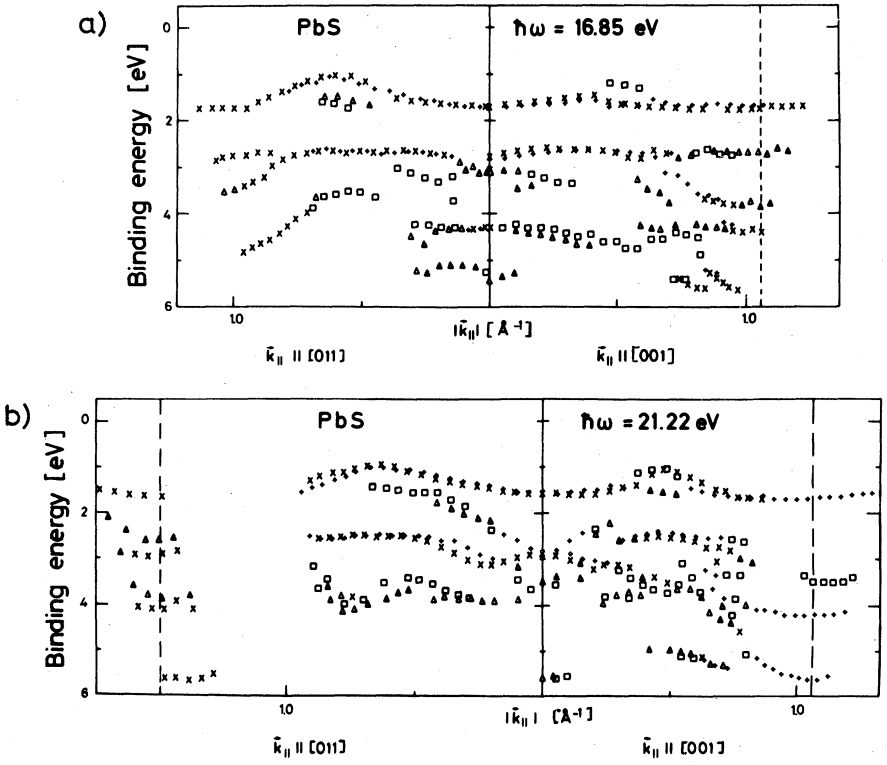


FIG. 4. (a) Peak positions vs momentum component $|\vec{k}_{\parallel}|$ obtained from the Ne I-excited angle-resolved photoemission spectra of PbS. (b) Same as (a) for the He I-excited spectra. No spectra have been taken around $|\vec{k}_{\parallel}| \simeq 1.1$ Å$^{-1}$ for $\vec{k}_{\parallel} \parallel [011]$.

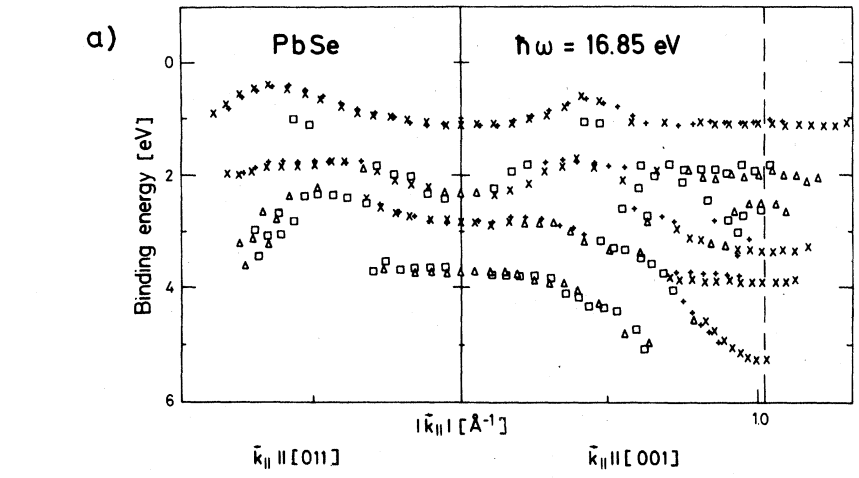


FIG. 5. Same as Fig. 4 for PbSe.

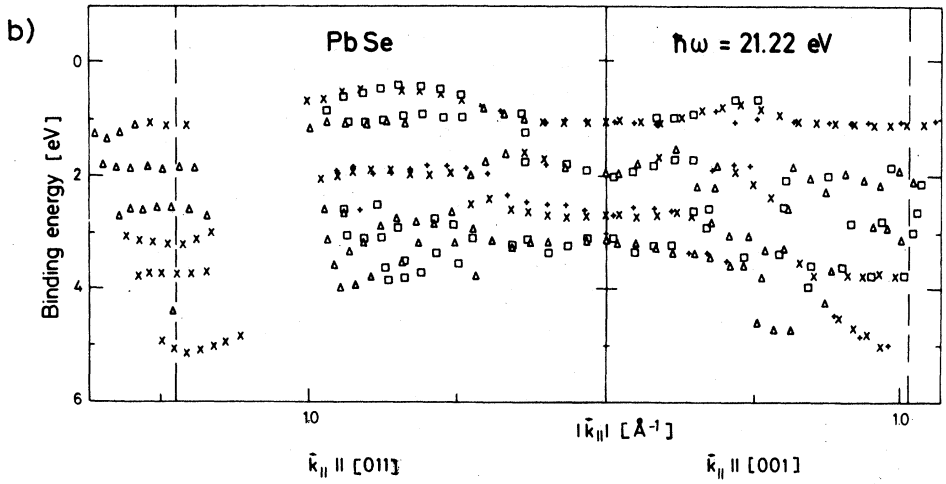


At $\vec{k}_{\parallel}=\vec{0}$ and around the zone boundaries sketched by vertical dashed lines, some of the $E$-vs-$\vec{k}_{\parallel}$ curves (to be imagined as continuously connecting the discrete data points) show distinct extrema. Noting the coincidence of these extrema with a zone center or a zone boundary in all lead salts and for both azimuthal orientations we suggest that they mirror the periodicity of the band structure in $\vec{k}$ space.

## IV. DISCUSSION

### A. One-dimensional density-of-states model

The first attempt to interpret the $E$-vs-$\vec{k}_{\parallel}$ plots of Figs. 4–6 has been based on the complete neglect of any selection rule concerning $k_{\perp}$.[49] This crude assumption could be justified by the overall (although not complete) similarity of the $E$-vs-$\vec{k}_{\parallel}$ plots for different photon energies, thus suggesting that final-state effects are not a main ingredient of angle-resolved photoemission from the lead salts. Consequently, all peaks in a spectrum for a given $\vec{k}_{\parallel}$ are tentatively identified with the peaks in the one-dimensional density of valence states along $k_{\perp}$ for fixed $\vec{k}_{\parallel}$. (Strictly speaking, angle-resolved photoemission spectra are recorded keeping $\sin\theta=|\vec{k}_{\parallel}|/\sqrt{2E}$ constant rather than $|\vec{k}_{\parallel}|$. Since, however, the factor $1/\sqrt{2E}$ is a slowly and monotonically varying function of $E$ in the relevant energy range and the observed peaks are very narrow, the positions of peaks should be practically the same in either case). A detailed comparison between the prediction of this one-dimensional density of states (ODDS) model with the experimental results will now be made for PbS.

The positions of lines in reciprocal space defined by $\vec{k}_{\parallel}=$const depend on the specific orientation of the sample relative to the acceptance cone of the electron analyzer. In Fig. 7 we have sketched the irreducible parts of these lines, within the

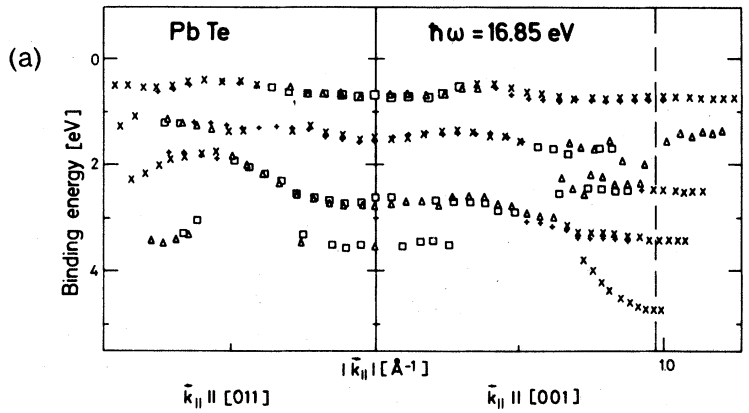


FIG. 6. Same as Fig. 4 for PbTe.

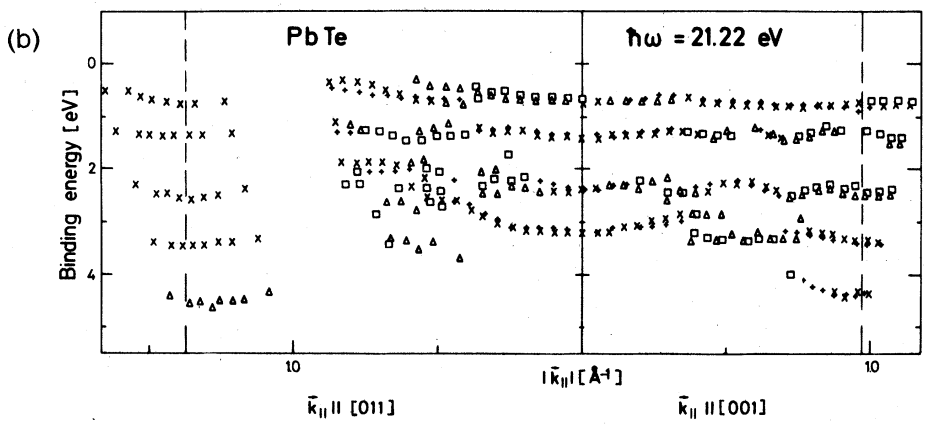


extended zone scheme of an fcc crystal, which correspond to the two different orientations used in our experiments. The one-dimensional density of states along these lines was calculated according to [cf. Eq. (9)]

$$D_1(E-\omega,\vec{k}_\parallel)\sim\sum_n\left|\frac{dE^{(n)}_{\vec{k}_\parallel,p_{\perp n}}}{dp_{\perp n}}\right|^{-1}_{E^{(n)}_{\vec{k}_\parallel,p_{\perp n}}=E-\omega}, \qquad (13)$$

with the summation extending over the three $p$-derived valence bands. The energy bands $E^{(n)}_{\vec{k}_\parallel,p_{\perp n}}$ were calculated utilizing the empirical pseudopotential method and the pseudopotential coefficients already employed by Kohn *et al.*[11] A spin-dependent term was included in the pseudopotential taking into account spin-orbit interaction.[54]

The energy dependence of the peaks in $D_1(E-\omega, \vec{k}_\parallel)$ is plotted as a function of $\vec{k}_\parallel$ in Fig. 8(a). We note that these peaks occur at the one-dimensional critical points or van Hove singularities in the band structure along $k_\perp$. Full lines in Fig. 8(a) correspond to critical points located at $k_\perp=0$, these lines are thus identical with the band struc-

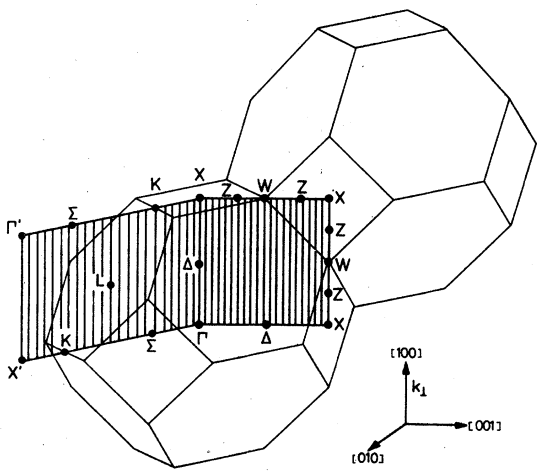


FIG. 7. Extended zone scheme of PbS. Our measurements were confined to wave vectors $\vec{k}$ lying (a) in the $\Gamma$-$X$-$X$-$X$ plane ($\vec{k}_\parallel \parallel [001]$), and (b) in the $\Gamma$-$X'$-$\Gamma'$-$X$ plane ($\vec{k}_\parallel \parallel [011]$). One-dimensional densities of states were calculated along $\vec{k}_\parallel$=const, as indicated by the vertical lines.

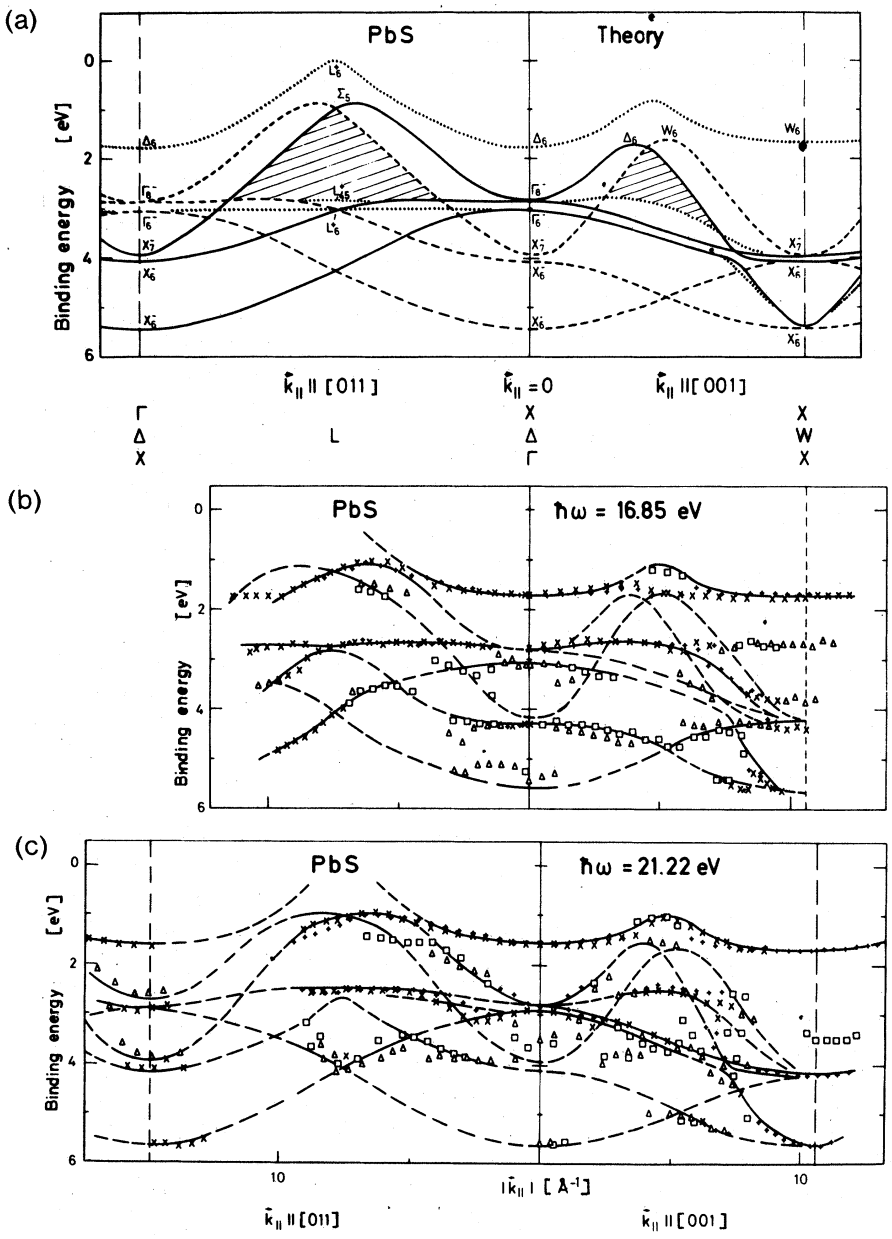


FIG. 8. (a) Dependence of the energies of critical points in the one-dimensional density of states on $\vec{k}_{\parallel}$. The solid lines refer to critical points at $k_{\perp}=0$, the dashed lines to critical points at $k_{\perp}=2\pi/a$, and the dotted lines to critical points at an intermediate value of $k_{\perp}$. The hatched areas represent band gaps within the $p$-derived valence bands. (b) and (c) Same as Figs. 4(a) and 4(b); the experimental points have now been connected to give energy vs momentum curves similar to shape to those of (a).

ture along $X'-K-\Sigma-\Gamma-\Delta-X$ (cf. Fig. 7). Dashed lines represent singularities at $k_{\perp}=2\pi/a$ (i.e., along the lines $\Gamma'-\Sigma-K-X-Z-W-Z-X$), and dotted lines to "accidental" critical points at an intermediate value of $k_{\perp}$. The shaded areas represent energy gaps within the $p$-type valence bands.

The experimental $E$-vs-$\vec{k}_{\parallel}$ plots for PbS (cf. Fig. 3) are shown again in Figs. 8(b) and 8(c), where we have connected the discrete data points by continuous lines similar to those predicted by the ODDS model [cf. Fig. 8(a)]. Thereby we are able to assign virtually all peaks observed in the angle-resolved photoemission spectra to critical points in the one-dimensional density of valence states. Some discrepancies between theory and experiment are observed at the zone boundary in the [001] direction for both photon energies. A possible explanation for the string of weak peaks at 2.7-eV binding energy in the Ne I-excited spectra could be a violation of the $\vec{k}_{\parallel}$ conservation: intense peaks are observed at the same energy, but at a different $|\vec{k}_{\parallel}| \simeq 0.5$ Å$^{-1}$. No satisfactory explanation can be given for the weak structures observed at 3.5 eV ($\hbar\omega=16.85$ eV) and 3.8 eV ($\hbar\omega=21.22$ eV) bind-

ing energy. At $\vec{k}_{\parallel}=\vec{0}$, our simple model fails to predict the shoulders observed at 3.5 eV ($\hbar\omega=$ 21.22 eV). All other disagreements between theory and experiment are to be regarded as minor.

The good overall agreement between theory and experiment in Fig. 8 lends substantial support to the assumption of nonconservation of the electron momentum component normal to the surface $k_{\perp}$ which has been made in the framework of the ODDS model. There are, however, two serious shortcomings of this model in addition to the few disagreements mentioned above. First of all, the ODDS model is not capable of predicting whether a given critical point will be observed as a peak in an experimental spectrum or not. Secondly, the experimental results are not as independent of the photon energy as the ODDS model predicts. In particular, the peak energies depend slightly on the photon energy: differences of ~ 0.2 eV may be deduced from a comparison of Figs. 8(b) and 8(c).

To summarize, there is clear evidence that final-state effects are yet present in the angle-resolved photoemission spectra for PbS and, more generally speaking, for all lead chalcogenides (cf. Figs. 4–6). Thus, we have to take into account the remnants of $k_{\perp}$ conservations in order to obtain a complete understanding of photoemission from these semiconductors. This will be the aim of Sec. IV B 1.

### B. Weighted-indirect-transition model

#### *1. Model calculations for normal emission*

In view of the complexity of the complete Eq. (9) for the differential photocurrent, we have adopted some simplifications in order to facilitate its numerical evaluation. First we have assumed that the reduced matrix elements $\bar{M}^{\pm}_{n''n}$ are constant and do not depend on the band indices $n$ and $n''$, the second assumption being more subtle than the first one. Although the quantities $\bar{M}^{\pm}_{n''n}$ are not expected to depend strongly on the energy for a given pair of bands $n$ and $n''$, they will depend on the symmetries of the initial and final states.

Moreover, we have not been able to calculate the valence-band structures on the basis of LEED theory, as it has been assumed in Sec. II A. Since relativistic effects are an important ingredient of the valence bands of at least PbSe and PbTe, such a calculation would have involved the relativistic LEED theory which is very complicated. Consequently we have not been able to determine the reflection coefficients $C_{nn'}(\vec{k}'_{\parallel}, E-\omega)$ [cf. Eq. (7)]. We have rather decided to approximate these quantities by $\delta(p_{\perp n}+p_{\perp n'})$, which is equivalent to replacing the true valence-band state by a standing wave consisting of two Bloch waves with opposite group velocities. The evanescent waves thus neglected are all characterized by $\partial[\mathrm{Re}(p_{\perp})]/\partial E \simeq 0$ in the energy range of interest. Transitions from these states into the similarly steep conduction bands could only give rise to a smooth background, especially if the smearing of the $p$-selection rule introduced by $\mathrm{Im}(p_{\perp})$ is taken into account. We must point out, however, that the mixing of propagating Bloch waves introduced by the surface is not treated exactly if there exist states with the same symmetry, but differend $|p_{\perp}|$, $p_{\perp}$ being real, at a given energy. This is the case for the uppermost valence band with $\Delta_1$ ($\Delta_6$) symmetry. While taking into account these effects in an appropriate manner could perhaps change the calculated spectra, these changes are not expected to be important as may be inferred from the good agreement between our calculations and experiments.

Finally, we have neglected the interference between the contributions to the differential photocurrent from different valence and conduction bands. Interference effects are important if large contributions to the differential photocurrent arise simultaneously from different bands; this is not the case in the course of the calculations presented below. The simplified version of Eq. (9) based on all these approximations is given by

$$j(\vec{R},E)\sim\sqrt{E}\sum_{n}\left|\frac{dE^{(n)}_{\vec{k}'_{\parallel},p_{\perp n}}}{dp_{\perp n}}\right|^{-1}_{E^{(n)}_{\vec{k}'_{\parallel},p_{\perp n}}=E-\omega}\times\sum_{n''}T_{n''}(\vec{k}_{\parallel},E)^2\left(\left|\frac{1}{1-\exp[i(p_{\perp n}-k^{*}_{n''})c_{\perp}]}\right|^2+\left|\frac{1}{1-\exp[i(-p_{\perp n}-k^{*}_{\perp n''})c_{\perp}]}\right|\right)^2 . \quad (14)$$

For calculating the transmission coefficients $T_{n''}(\vec{k}_{\parallel},E)$, the weak influence of the potential barrier at the surface has been neglected. The atomic scattering phase shifts needed as input parameters for the LEED theory have been calculated using relativistic APW potentials for PbS, PbSe, and PbTe.[55] The resulting relativistic phase shifts have been averaged according to the statistical

branching ratios:

$$\bar{\delta}_l = [(l+1)\delta_{l+\frac{1}{2}} + l\,\delta_{l-\frac{1}{2}}]/(2l+1)\,. \quad (15)$$

The phase shifts thus obtained still include the mass-velocity and Darwin corrections, which may still be important at ~20 eV above the muffin-tin zero. On the other hand, spin-orbit splittings are expected to be small in this energy range. Therefore the neglect of spin-orbit interaction should not represent a major shortcoming of our calculations.

As has been pointed out above, the same approximation is invalid in the case of the valence bands. Instead, the following procedure has been adopted to calculate the valence-band structures: (i) Calculate the band structure using the empirical-pseudopotential method and pseudopotential coefficients published elsewhere,[11,25] but without taking into account spin-orbit interaction; (ii) reobtain these results by using a tight-binding Hamiltonian of the Slater-Koster-type[56] and by adjusting the parameters of this Hamiltonian, and (iii) finally include the spin-orbit interaction into the tight-binding Hamiltonian.[57] The main advantage of this technique as compared with the empirical-pseudopotential method is that it requires far less computational time.

In order to obtain a common energy scale for the valence and the conduction bands thus calculated from different potentials, we have calculated the energy of the valence bands at point $\Gamma$ by using the relativistic APW potential as well. The results of the tight-binding calculation have then been fitted to the APW result by adding a constant potential.

Reliable information concerning the imaginary part $V_{oi}$ of the complex inner potential that represents the finite lifetime of the hot electron may be taken from earlier applications of the theory of LEED.[32] Commonly used values are −4 eV above the plasmon threshold $\hbar\omega_p$ and −1 eV between the Fermi energy and the plasmon energy. The transition in the region of the plasmon threshold has been approximated by a Fermi-Dirac function with a width of 2 eV

$$V_{oi}(E) = -1.0 - 3.0/\{1.0 + \exp[-(E - E_F - \hbar\omega_p)/0.68]\}\ \text{eV}\,. \quad (16)$$

The plasmon energies may be deduced from electron energy-loss experiments[13,14] or x-ray induced photoelectron spectroscopy.[18] We have used 15.5, 15.3, and 14.8 eV for PbS, PbSe, and PbTe, respectively. The Fermi level $E_F$ was taken to lie in the middle of the very small fundamental gap.

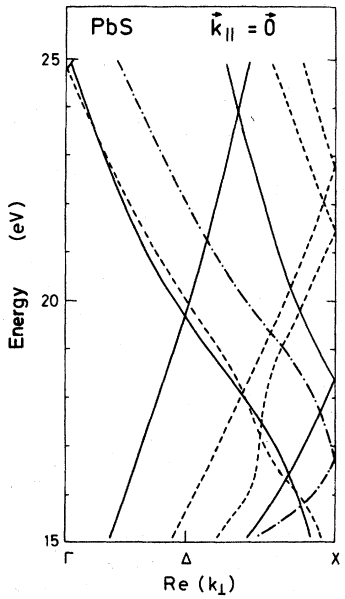


FIG. 9. Complex conduction-band structure of PbS. Only the real part of the complex wave-vector component $k_\perp$ is shown here. The significance of the different representations of the bands is explained in the text.

### 2. *Results and comparison with experiment*

In Fig. 9, we present the complex conduction-band structure [only the real part of $k_\perp(\vec{k}_{\parallel}, E)$ is shown in this figure] of PbS for $\vec{k}_{\parallel} = \vec{O}$ which has been calculated in the relevant energy range by using the layer-KKR method. We first discuss some of its general properties that allow a qualitative understanding of some aspects of angle-resolved photoemission.

First, we note that only those bands represented by solid lines couple to the plane wave outside the crystal, for all other bands we obtain $T_{n''}(\vec{k}_{\parallel} = \vec{O}, E) \equiv 0$. This result is a direct consequence of the symmetry of the crystal surface. As Hermanson has pointed out,[58] the final state encountered in photoemission transforms like the fully symmetric irreducible representation of the appropriate space group. In the special case of normal emission from the (100) surface of a fcc crystal the space group is $C_{4v}$, and the final state of photoemission has $\Delta_1$ symmetry. Thus, only the bands with $\Delta_1$ symmetry entry the expansion of the final state $\phi(\vec{r}, \vec{R}, E)$ into Bloch waves [cf. Eqs. (3a) and (6)]. The "expansion coefficients" $T_{n''}(\vec{O}, E)$ for all bands with other symmetries, represented by the dashed and dashed-dotted lines in Fig. 9, must vanish identically.

No such strict selection rule applies to the allowed conduction bands if $\vec{k}_{\parallel} \neq \vec{O}$. For $\vec{k}_{\parallel} \parallel [001]$ or $\vec{k}_{\parallel} \parallel [011]$ the only nontrivial symmetry operation present is the mirror symmetry about the plane

defined by $\vec{k}_{\parallel}$ and the surface normal, hence the designation "mirror plane" emission applies to this situation. The final state needs only be even with respect to this mirror plane. If we choose $\vec{k}_{\parallel} = (2\pi/a)(0, 1, 1)$, the band structure is the same as for $\vec{k}_{\parallel} = \vec{O}$, except for the replacement $k_{\perp} \rightarrow 2\pi/a - k_{\perp}$, see Fig. 7. Yet the number of allowed conduction bands is considerably higher, since bands represented by full or dashed lines are even. The dashed-dotted line represents the only odd band present.

This important difference between normal and mirror plane emission sheds some light upon the question of which of the proposed simple models of angle-resolved photoemission is more appropriate, either the direct transition model or the ODDS model. Normal emission corresponds to the smallest number of available conduction bands, thus final-state effects (i.e., effects of a residual $k_{\perp}$-selection rule) should most probably be observed in this configuration. Nearly all recent angle-resolved photoemission experiments[34,35,39,40,42,43,47] have been carried out for $\vec{k}_{\parallel} = \vec{O}$. Consequently it is not surprising that most of these experiments have successfully been interpreted on the basis of $k_{\perp}$-conserving direct transitions.

On the other hand, most of the measurements on the lead salts reported by the present authors[49] have been performed utilizing mirror plane emission, resulting in a considerably larger number of available conduction bands. A further increase of this number (e.g., compared to the noble metals) is due to the fact that the Brillouin zones of the lead salts ($a_0 \simeq 6$–$6.5$ Å) are smaller than those of the noble metals ($a_0 \simeq 3$–$4$ Å). In addition, the same absolute amount of $k_{\perp}$ broadening will have more importance in a crystal with a small Brillouin zone than in a crystal with a large one. As a natural consequence of all these effects, the assumption of continuous and dense final states may be a good approximation in the case of the lead salts. This accounts for the good agreement between the experimental results and the prediction of the ODDS model. Possibly the same holds for the results obtained on Bi(0001).[46]

Since final-state effects are expected to be most important for normal photoemission (i.e., $\vec{k}_{\parallel} = \vec{O}$), we have calculated angle-resolved photoemission spectra of PbS according to Eq. (14) only for this case. The resulting spectra have been convoluted with a Gaussian with a full width at half-maximum of 0.3 eV in order to simulate the energy resolution of the analyzer, the effect of finite (but nevertheless very high) angular resolution was neglected. The results are shown for the two different photon energies in Fig. 10(b), the underlying band structure is shown in Fig. 10(c). The three $p$-derived valence bands have been shifted by $\hbar\omega$ towards higher energies. The conduction band represented by a full line couples most strongly to the plane wave outside the crystal. The amplitudes $T_{n''}(\vec{O}, E)$ of the other two conduction bands only amount to 20% and 5% of the amplitude of the dominant one. Since the square of the amplitude enters the Eq. (14) for the differential photocurrent, the contributions of the latter two bands to the total spectra are rather small [see the dashed lines in Fig. 10(b)].

Comparing the calculated spectra with the experimental results shown in Fig. 10(a), we first emphasize that all theoretically predicted peaks

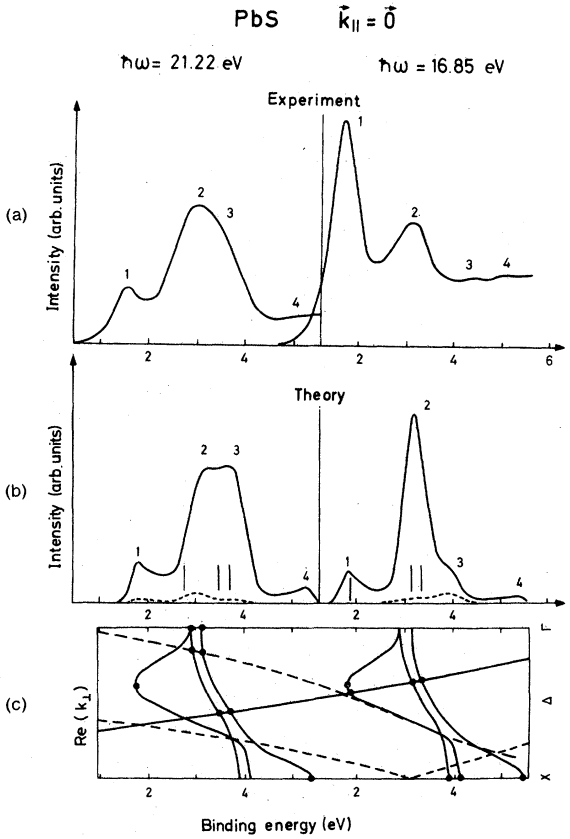


FIG. 10. Angle-resolved photoemission from PbS for $\vec{k}_{\parallel} = \vec{0}$. (a) Experimental spectra; (b) calculated spectra; vertical bars denote possible direct transitions into the most important conduction band. The contribution to the total photocurrent that is due to the two other conduction bands is shown by dashed lines; (c) band structure: The three $p$-derived valence bands have been shifted towards higher energies by the respective photon energy. That conduction band shown by a full line couples strongly, those shown by dashed lines couple only weakly to the plane wave in the vacuum region. The dots denote those direct transitions and one-dimensional critical points that give rise to peaks.

TABLE I. Experimental and theoretical binding energies (eV) of peaks in the normal emission spectra of PbS.

| Photon energy (eV) | Peak No. (cf. Fig. 10) | $E_B$ (experiment) | $E_B$ (theory) |
|---|---|---|---|
| 16.85 (Ne I) | 1 | 1.7 | 1.8 |
| | 2 | 2.8<br>3.1 | 3.1 |
| | 3 | 4.3 (weak) | 3.9 (shoulder) |
| | 4 | 5.3 (weak) | 5.3 (weak) |
| 21.22 (He I) | 1 | 1.6 | 1.8 |
| | 2 | 2.9 | 3.3 |
| | 3 | 3.5 (shoulder) | 3.6 |
| | 4 | 5.4 (weak) | 5.3 (weak) |

are actually observed in the experimental spectra. Thus, one of the main shortcomings of the ODDS model is being avoided by the improved model. Experimental and calculated binding energies are compared in Table I. The agreement between theory and experiment is very good even for the weakest observed structures. The splitting of peak 2 in the NeI-excited spectrum has been taken from the second derivative, thus it is not apparent in Fig. 10(a).

The calculated peaks may be identified with direct transitions or critical points in the one-dimensional density of valence states. Direct optical transitions into the most important conduction band may occur at the energies marked by vertical bars in Fig. 10(b). The only direct transition that does not result in a peak is located at 2.75-eV binding energy in the HeI-induced spectrum. The corresponding peak is too weak to be observed because the one-dimensional density of states of the participating valence is too low, the band is too steep. On the other hand, all those peaks that are not the result of direct transitions may be identified with singularities in the one-dimensional density of valence states. These singularities can give rise to peaks only as a result of the relaxation of the $k_\perp$ conservation. A typical example is peak 1 in the HeI-induced spectrum. In case that no conduction band with a sufficient amplitude is close enough to the critical points, the resulting peak may not or hardly be observable in the spectrum (e.g., peak 4 in the NeI-excited spectrum).

Thus, we have obtained clear evidence for indirect (peak 1 in the HeI-induced spectrum) as well as for direct (peak 3 in the same spectrum) transitions in the angle-resolved photoemission spectra of PbS. Nevertheless some peaks contain contributions from both direct and indirect transitions, e.g., peak 2 in the NeI-excited spectra. In Fig. 11 curve (a) represents the same peak on an expanded energy scale while curve (b) shows the same region of the spectrum before the convolution with the Gaussian. In the latter curve we realize two rather broad structures arising from direct transitions (vertical bars) and two very sharp peaks which are due to singularities in the one-dimensional density of states. Due to finite experimental resolution and possibly to some extent also due to thermal broadening effects, a single peak is observed in the experiment.

However, rigorously speaking, purely direct or indirect transitions occur only in the limits of vanishing and infinitely strong damping, respectively. Assuming the more realistic case of some finite damping, direct and indirect transitions from all occupied states contribute to the spectra.

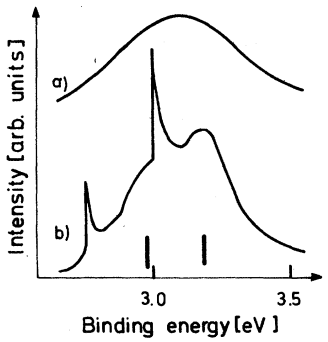


FIG. 11. (a) Enlarged section (peak 2) of the NeI-excited ($\hbar\omega = 16.85$ eV) calculated spectrum shown in Fig. 10(b). (b) Same as (a) before the convolution with the Gaussian. The vertical bars represent direct transitions.

Contributions from indirect transitions are, however, to be weighted according to the relaxed $k_\perp$ selection rule [cf. Eq. (14)]. Thus, we propose to call the model presented in this article the "weighted indirect transitions model." Yet we are still able to relate peaks to characteristic properties of the band structure by identifying them as the result of either direct or indirect transitions.

The intensities of nearly all peaks are reproduced with reasonable accuracy by our calculations, the only serious deviation is related to peak 1 in the NeI-excited spectrum (cf. Fig. 10). Probably this disagreement between theory and experiment is due to the neglect of the reduced matrix elements in Eq. (14), which is the basis of our model calculations. These reduced matrix elements depend on the symmetries of the wave functions involved. The symmetry of the initial state for peak 1 is different from that for peak 2 ($\Delta_1$ vs $\Delta_5$, respectively, in single-group notation). The neglect of this difference in our calculations could account for the wrong relative intensities of peaks 1 and 2 in the calculated NeI-excited spectrum.

In Figs. 12 and 13 we present the corresponding results for PbSe and PbTe. A comparison of theoretical and experimental peak energies is supplied in Tables II and III. We obtain similar agreement as for PbS with respect to peak energies and again some discrepancies concerning the peak intensities, especially in the NeI-excited spectra. The calculated binding energies of peak 3 and 4 in the spectra of PbTe are too small by ~0.6 eV. This disagreement suggests that the EPM valence-band structure of PbTe (see Ref. 25) employed here is wrong in the region around the $X$ point. A similar result will be obtained in Sec. IV D.

Finally we emphasize that the main contributions to the normal emission spectra are due to only one conduction band in the case of all three lead salts. The contributions of the other conduction bands shown by dashed lines are perhaps present (at least in the case of PbS), but not important. Moreover, the dispersion of the main conduction band may be calculated from the relation $E = \frac{1}{2}k^2/\alpha + V_0^*$, where $\alpha$ is an effective-mass parameter equal to $m_0^*/m_0$. For PbS, we obtain $\alpha = 1.1$ and $V_0^* = 3.3$ eV (referred to the muffin-tin zero) by fitting the nearly free-electron parabola to the calculated conduction band between 15 and 25 eV. It must be noted that in view of the steepness of the conduction band the energetic positions of pos-

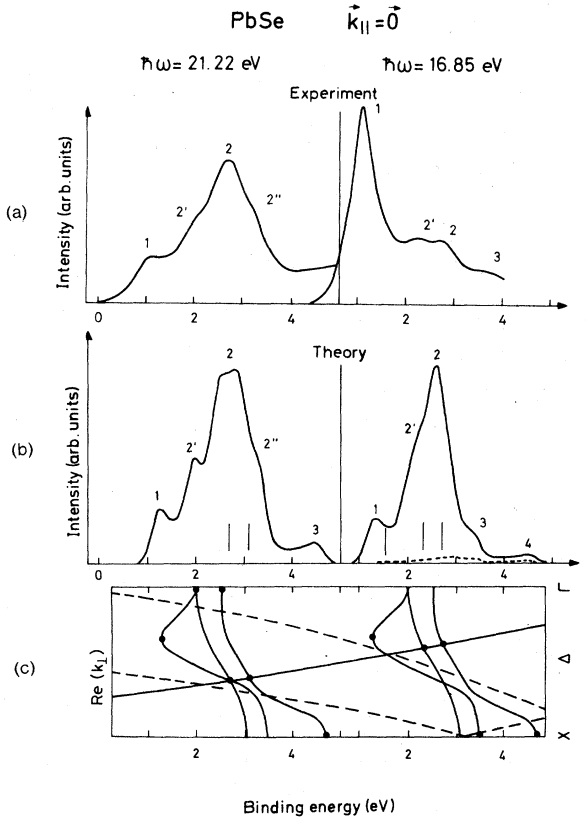


FIG. 12. Same as Fig. 10 for PbSe.

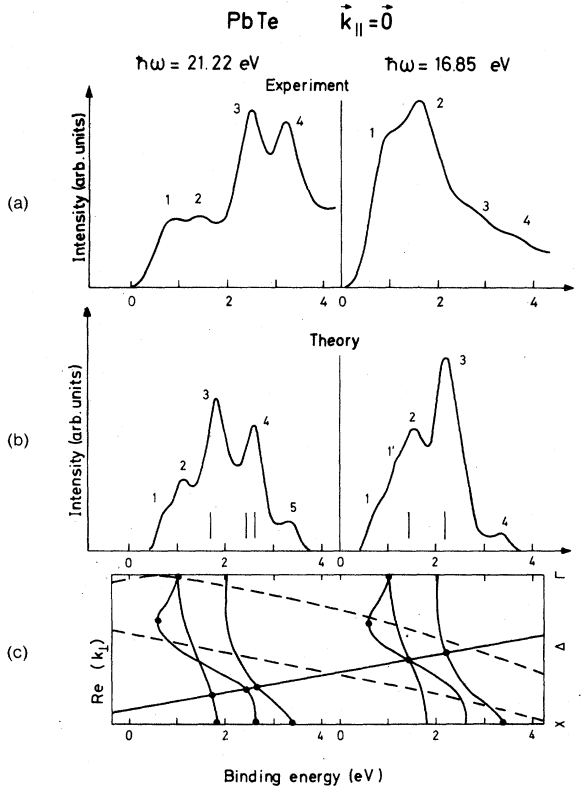


Fig. 13. Same as Fig. 10 for PbTe.

TABLE II. Experimental and theoretical binding energies (eV) of peaks in the normal emission spectra of PbSe.

| Photon energy (eV) | Peak No. (cf. Fig. 12) | $E_B$ (experiment) | $E_B$ (theory) |
|---|---|---|---|
| 16.85 (Ne I) | 1 | $1.0_5$ | 1.3 |
| | 2′ | $2.2_5$ | 2.1 (shoulder) |
| | 2 | $2.7_5$ | 2.6 |
| | 3 | 3.6 (weak) | 3.4 (shoulder) |
| | 4 | ••• | 4.5 (weak) |
| 21.22 (He I) | 1 | $1.0_5$ | 1.3 |
| | 2′ | 1.9 (shoulder) | 2.0 |
| | 2 | 2.7 | 2.6 (shoulder)<br>2.9 |
| | 2′′ | 3.2 (shoulder) | 3.4 (shoulder) |
| | 3 | ••• | 4.5 (weak) |

sible direct transitions are drastically affected by seemingly small variations of $\alpha$.

Thus it is not surprising that reasonable angle-resolved photoemission spectra may be calculated on the basis of the single plane-wave approximation to the final state. One has, however, to take into account momentum-broadening effects, i.e., introduce an imaginary part of $k_\perp$. Yet the virtually good agreement between such a simple model and experimental results that has been achieved for copper[59] suffers from the existence of two adjusted parameters $(\alpha, V_0^*)$ that enter the calculations. On the other hand, the calculations presented here and more elaborate ones concerning copper[5,48] and molybdenum[48] do not contain any empirical parameter that has been adjusted in order to reproduce the angle-resolved photoemission spectra. Consequently, agreement between theory and experiment should bear more significance in the latter cases.

### C. Matrix elements and valence-band symmetries

So far, we have only utilized the information about the band structures that is related to the peak *energies*. Since the evaluation of the reduced matrix elements (in the following we shall omit the term "reduced" for simplicity) is rather involved, it is more difficult to make use of the informations contained in the peak *intensities*. However,

TABLE III. Experimental and theoretical binding energies (eV) of peaks in the normal emission spectra of PbTe.

| Photon energy (eV) | Peak No. (cf. Fig. 13) | $E_B$ (experiment) | $E_B$ (theory) |
|---|---|---|---|
| 16.85 (Ne I) | 1 | 0.7 (shoulder) | 0.7 (shoulders) |
| | 1′ | | 1.1 |
| | 2 | 1.5 | 1.5 |
| | 3 | 2.8 (shoulder) | 2.2 |
| | 4 | 3.5 (weak) | 3.3 |
| 21.22 (He I) | 1 | $0.7_5$ | 0.7 (shoulder) |
| | 2 | 1.4 | 1.1 |
| | 3 | 2.5 | 1.8 |
| | 4 | 3.2 | 2.6 |
| | 5 | ••• | 3.3 (weak) |

the dependence of a matrix element on the angle of incidence of the light $\theta_\omega$ is completely determined by the symmetries of the initial and final states, if all other experimental parameters ($\hbar\omega, \theta$ etc.) are kept constant. Consequently, it is possible to obtain information about the symmetries of the participating wave functions without explicitly calculating the matrix elements, if one measures the intensity $j$ of a given peak as a function of the angle $\theta_\omega$.

Scheffler *et al.*[60] have derived the functions $j(\theta_\omega)$ for normal photoemission from a fcc crystal. For emission from valence states with $\Delta_1$ symmetry ($p_z$-like) they obtain

$$j_{\Delta_1}(\theta_\omega) \sim |1+r_p(\theta_\omega)|^2 \sin^2\theta_\omega\,, \tag{17}$$

while the corresponding expression for states with $\Delta_5$ symmetry ($p_x, p_y$-like) is

$$j_{\Delta_5}(\theta_\omega) \sim |1+r_s(\theta_\omega)|^2 + |1-r_p(\theta_\omega)|^2 \cos^2\theta_\omega\,. \tag{18}$$

Normal photoemission from states with symmetries different than $\Delta_1$ or $\Delta_5$ is forbidden on account of selection rules.[58] $r_s$ and $r_p$ are the complex reflectivities for $s$- and $p$-polarized light.

Inserting these quantities from Fresnel's formula, we obtain no emission ($j_{\Delta_1}=0$) from states with $\Delta_1$ symmetry at normal incidence [$\theta_\omega = 0°$, $r_s(0°)=1$; $r_p(0°)=0$], while $j_{\Delta_5}$ reaches its maximum for these incidence conditions. For $\theta_\omega = 90°$ (grazing incidence), we obtain vanishing emission in either case [$r_s(90°)=-1$; $r_p(90°)=-1$].

It has, however, to be questioned whether these results are applicable to the lead salts, since energy bands with symmetries $\Delta_1$ and $\Delta_5$ mix heavily through spin-orbit interaction in these materials. A simplified valence-band structure of PbS that does not take into account the spin-orbit interaction is shown schematically in Fig. 14(a). The $p$-type valence bands considered in our work consist of a doubly degenerate band with $\Delta_5$ symmetry and a nondegenerate band with $\Delta_1$ symmetry. The more realistic band structure based on double-group symmetries is shown in Fig. 14(b). We note that on account of spin-orbit interaction the double degeneracy of the band with $\Delta_5$ symmetry is lifted, and two nondegenerate bands with the symmetries $\Delta_6$ and $\Delta_7$ arise. The bands with $\Delta_1$ symmetry remain nondegenerate, now with $\Delta_6$ symmetry.

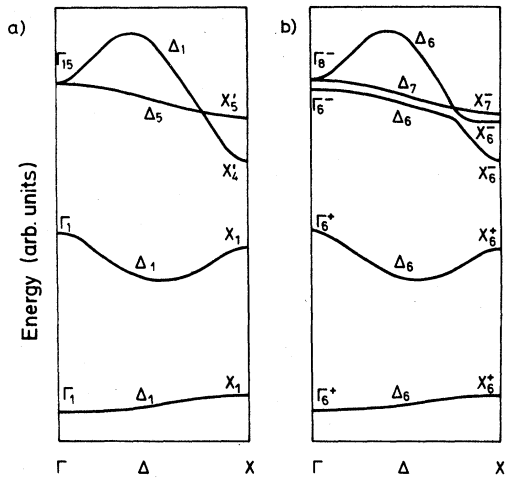


FIG. 14. Schematic valence-band structure of PbS along the line Δ. (a) without, (b) with taking into account the spin-orbit interaction.

We emphasize that only one component of the doubly degenerate state with $\Delta_5$ symmetry is mixed with states with $\Delta_1$ symmetry. That component which transforms into the band with $\Delta_7$ symmetry remains unmixed, unless another band, e.g., with the symmetry $\Delta_{2'}$, is present nearby. Such a band only exists in the conduction bands of the lead salts and is separated by 7–12 eV from

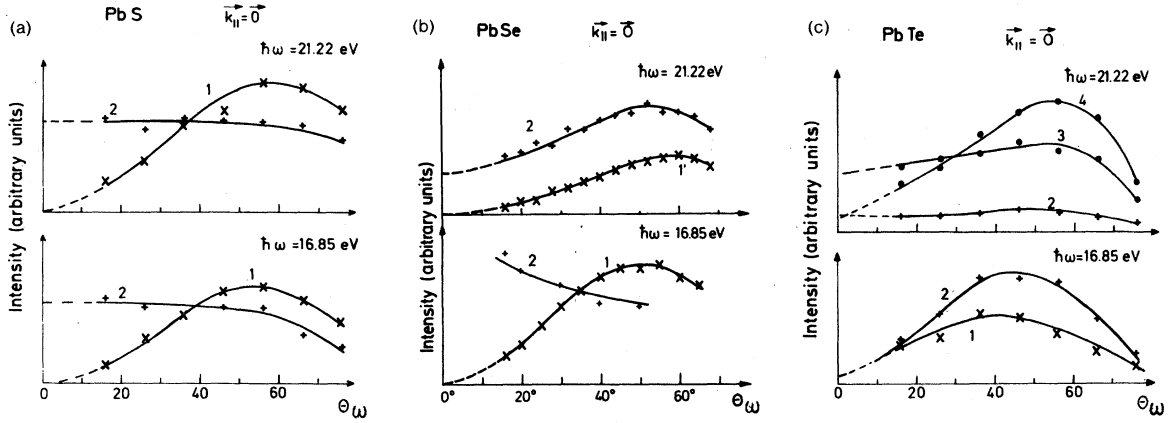


FIG. 15. Peak intensities in angle-resolved normal emission spectra as depending on the photon incidence angle $\theta_\omega$. (a) PbS (The numbering of peaks refers to Fig. 10.) (b) PbSe (cf. Fig. 12). (c) PbTe (cf. Fig. 13).

the valence bands along the line $\Delta$ (cf. Fig. 1). Consequently, Eq. (18) should be applicable to valence bands with $\Delta_5$ ($\Delta_7$) symmetry even in the case of strong spin-orbit interaction. On the other hand, the emission intensities from valence bands with the symmetries $\Delta_1$ ($\Delta_6$) and $\Delta_5$ ($\Delta_6$) may be calculated according to the Eqs. (17) and (18) probably only in the limit of weak spin-orbit interaction.

The experimental results for all three lead salts are displayed in Fig. 15. The $j(\theta_\omega)$ curves obtained for PbS may readily be used to identify peaks 1 and 2 with initial states with the symmetries $\Delta_1$ ($\Delta_6$) and $\Delta_5$ ($\Delta_6, \Delta_7$), respectively. This identification is consistent with that based on the weighted indirect transition model (cf. Fig. 10).

The results obtained for PbSe permit the same straightforward interpretation only for $\hbar\omega = 16.85$ eV, as may be seen in Fig. 15(b). For $\hbar\omega = 21.22$ eV, peak 1 may likewise be identified with an initial state with $\Delta_1$ ($\Delta_6$) symmetry, while peak 2 rather shows a complex behavior. This peak actually consists of three components, which are not easily deconvoluted. Figure 12 shows that these components are related to valence bands with different symmetries, in agreement with the fact that the $j(\theta_\omega)$ curve of peak 2 can be described neither by Eq. (17) nor by Eq. (18).

No information concerning the initial-state symmetries is obtainable in the case of PbTe [see Fig. 15(c)]. We note that both peaks in the NeI-induced ($\hbar\omega = 16.85$ eV) spectrum arise from valence bands with different symmetries, the same holds for peak 4 in the HeI-induced spectrum (cf. Fig. 13). Peaks 2 and 3 in the latter spectrum should arise from valence bands with symmetry $\Delta_7$, as may be seen in Fig. 13. Actually the intensity variations of both peaks are not very different from that predicted by Eq. (18). The observed deviations might be due to uncertainties in the deconvolution procedure that has been used to obtain the intensities of these peaks and to the possibly doubtful extrapolation for $\theta_\omega \to 0°$.

In conclusion, the measurement of peak intensities as a function of the light incidence angle has in some cases revealed the symmetry of the corresponding initial state. In any case, the results obtained in this context are consistent with the assignments of peaks to valence bands based on the weighted indirect transition model.

### D. Comparison with various band-structure calculations

#### *1. Binding energies of representative critical points*

As we have pointed out in the last section, the peaks in angle-resolved photoemission spectra are in many cases related to singularities in the one-dimensional density of valence states calculated along $k_\perp$ for fixed $\vec{k}_\parallel$. Final-state effects related to a smeared out conservation of $k_\perp$ may cause small shifts of the peak energies, suppress peaks predicted by the ODDS model or in few cases even give rise to additional peaks, but these effects are expected to be important only in the case of normal emission. This hypothesis is corroborated by the fact that around $\vec{k}_\parallel = 1.5(0, 1, 1)$ Å$^{-1}$ all peaks predicted by the ODDS model appear in the $E$-vs-$\vec{k}_\parallel$ curves of PbS [cf. Figs. 8(a) and 8(c)]. Consequently, final-state effects may be neglected for emission in a mirror plane to a good approximation and binding energies of three-dimensional critical points in the valence bands may be taken directly from the experimental $E$-vs-$\vec{k}_\parallel$ plots.

The positions of three-dimensional critical points in the $E$-vs-$\vec{k}_\parallel$ curves are indicated in Fig. 8(a). The experimental binding energies $E_B$ (referred to the Fermi energy) of these critical points as obtained from Figs. 5, 6, and 8 are compiled in Table IV. We did not employ the experimental $E$-vs-$\vec{k}_\parallel$ plots in the region of $\vec{k}_\parallel \simeq \vec{0}$ for the reasons outlined above. We have also listed the total width $\Delta E$ of the $p$-type valence bands at $\vec{k}_\parallel = (2\pi/a)(0, 0, 1)$ [$\Delta E = E(W_6) - E(X_6^-)$, cf. Fig. 8(a)], and at $\vec{k}_\parallel = (2\pi/a)(0, 1, 1)$ [$\Delta E = E(\Delta_6) - E(X_6^-)$] as well as the energy gap $E_g$ within the $p$-type valence bands at $\vec{k}_\parallel = (2\pi/a)(0, \frac{1}{2}, \frac{1}{2})$ [$E_g = E(\Sigma_5$ at $(2\pi/a)(0, \frac{1}{2}, \frac{1}{2})) - E(L_{45}^+)$].

In Table IV, the experimental values obtained for $E_B$, $\Delta E$, and $E_g$ are compared with the results of four different band-structure calculations (cf. Fig. 1 for a typical band structure). These are two empirically adjusted pseudopotential calculations using a local[11,25] and nonlocal[26] pseudopotential, and a relativistic OPW calculation[20] containing no adjustable parameter. The fourth theoretical entry is a relativistic APW calculation,[55] which treats the constant potential between the muffin-tin spheres as an adjustable parameter in order to fit the fundamental energy gap.

Before comparing the theoretical and experimental results in detail we have to observe that the calculated binding energies are referred to the top of the valence bands, while the measured binding energies are referred to the Fermi level. The two reference energies may deviate from each other by 0.2–0.3 eV, this may introduce systematic discrepancies between all calculated and measured binding energies in Table IV. However, the quantities $\Delta E$ and $E_g$, representing energy differences between well-defined critical points, do not depend on any reference energy.

In PbS, the experimental values for the total bandwidths and the energy gap agree quite well with the predictions of the APW and (as far as

TABLE IV. Experimental (referred to the Fermi level) and calculated (referred to the top of the valence bands) binding energies of three-dimensional critical in the valence bands of the lead salts.[a]

| Symmetry designation | PbS | | | | | PbSe | | | | | | PbTe | | | | | |
|---|---|---|---|---|---|---|---|---|---|---|---|---|---|---|---|---|---|
| | Experiment | | Theory | | | Experiment | | Theory | | | | Experiment | | Theory | | | |
| | Ne I | He I | EPM[b] | OPW[c] | APW[d] | Ne I | He I | EPM[b] | EPM[e] | OPW[c] | APW[d] | Ne I | He I | EPM[f] | EPM[e] | OPW[c] | APW[d] |
| $\Gamma_8^-$ | ••• | $2.5_5$ | 2.87 | 2.57 | 2.46 | ••• | $1.8_7$ | 2.0 | $1.8_5$ | 2.03 | 1.83 | ••• | $1.3_5$ | 1.0 | $0.9_5$ | 1.12 | 0.88 |
| $\Gamma_6^-$ | ••• | $2.8_5$ | 3.09 | 2.83 | 2.70 | ••• | $2.5_4$ | $2.5_5$ | 2.4 | 2.58 | 2.43 | ••• | $2.5_5$ | 2.1 | 2.0 | 2.15 | 1.98 |
| $X_7^-$ | (3.8) | $3.8_9$ | 3.95 | 3.49 | 3.45 | $3.2_2$ | $3.2_2$ | $3.2_5$ | 3.9 | 3.13 | 2.99 | 2.5 | $2.5_5$ | 2.1 | 2.7 | 2.44 | 2.37 |
| $X_6^-$ | $4.3_8$ | $4.1_1$ | 4.09 | 3.74 | 3.68 | $3.7_8$ | $3.7_4$ | 3.6 | $4.2_5$ | 3.55 | 3.43 | $3.4_5$ | $3.4_5$ | 2.8 | 3.3 | 3.11 | 3.06 |
| $X_6^-$ | (5.7) | $5.6_5$ | 5.44 | 5.24 | 5.26 | $5.1_6$ | $5.1_6$ | 4.9 | $6.4_5$ | 4.89 | 4.94 | $4.7_5$ | $4.5_5$ | $3.7_5$ | 4.6 | 4.34 | 4.63 |
| $W_6$ | $1.6_8$ | $1.6_8$ | 1.66 | ••• | 1.30 | $1.0_1$ | $1.0_8$ | ••• | ••• | ••• | 0.98 | $0.7_5$ | $0.7_5$ | ••• | ••• | ••• | 0.40 |
| $L_{45}^+$ | 2.7 | $2.5_1$ | 2.90 | 2.32 | 2.22 | 2.0? | 1.9? | 2.2 | 2.1 | 1.86 | 1.61 | 1.2 | $1.2_5$ | 0.9 | 1.3 | 0.95 | 0.71 |
| $L_6^+$ | ••• | ••• | 2.99 | 2.36 | 2.25 | ••• | ••• | 2.6 | 2.2 | 2.08 | 1.38 | $1.8_5$ | 1.9 | $2.0_5$ | 1.7 | 1.53 | 1.36 |
| $\Delta_6$(max.) | $1.6_8$ | $1.5_7$ | 1.76 | ••• | 1.39 | $1.0_5$ | $1.1_2$ | $1.1_5$ | $0.7_5$ | ••• | 1.03 | $0.7_1$ | $0.7_5$ | 0.6 | $0.3_5$ | ••• | 0.33 |
| $\sum_5$(max.) | $1.0_5$ | 1.0 | 0.93 | ••• | 0.52 | 0.4 | $0.4_5$ | $0.5_5$ | 0.3 | ••• | 0.37 | 0.4 | 0.3 | 0.3 | $0.2_5$ | ••• | 0.04 |
| $\Delta E((2\pi/a)(0,0,1))$ | (4.0) | 4.0 | 3.78 | ••• | 3.96 | 4.2 | (4.1) | ••• | ••• | ••• | 3.96 | 4.0 | 3.8 | ••• | ••• | ••• | 4.23 |
| $\Delta E((2\pi/a)(0,1,1))$ | ••• | 4.0 | 3.68 | ••• | 3.87 | ••• | 4.0 | $3.7_5$ | 5.7 | ••• | 3.91 | ••• | 3.8 | $3.1_5$ | $4.2_5$ | ••• | 4.30 |
| $E_g((2\pi/a)(0,\frac{1}{2},\frac{1}{2}))$ | $1.4_5$ | $1.3_5$ | 1.90 | 1.4 | 1.62 | (1.4) | 0.9 | $1.4_5$ | 1.2 | 1.0 | 1.03 | 0.6 | $0.6_5$ | 0.4 | $0.6_5$ | 0.4 | 0.20 |

[a] EPM results for PbSe and PbTe have been taken from the figures in Refs. 11 and 26.
[b] Reference 11.
[c] Reference 20.
[d] Reference 55.
[e] Reference 26.
[f] Reference 25.

available) the OPW calculations. In contrast the EPM calculation by Kohn *et al.* predicts band widths which are too small by 0.2 to 0.3 eV, while the energy gap at $\vec{k}_{\parallel} = (2\pi/a)(0, \frac{1}{2}, \frac{1}{2})$ is too large by 0.5 eV. The calculation of this energy gap involves the binding energies of the uppermost valence band ($\Sigma_5$) at $\vec{k} = (2\pi/a)(0, \frac{1}{2}, \frac{1}{2})$ and the fourth valence band at point $L$ ($L_{45}^{+}$). Only the second of these energy levels represents a three-dimensional critical point that may give rise to significant structure in reflectivity spectra. Thus, the energy difference between the two levels is essentially a result of an interpolation which is inherent in every EPM calculation. The deviation between the EPM calculation on one hand and the calculation as well as the experimental results for $E_g$ on the other hand tells us that this interpolation may produce errors of the order of 0.5 eV.

Comparing the experimental and theoretical results for various critical points we note that the OPW and APW calculations predict binding energies which are systematically too small by ~ 0.3–0.4 eV. Bearing in mind the different reference energies employed in the calculations and experiments and the otherwise good agreement between the OPW and APW calculations and the experimental results, we tend to conclude that the Fermi level was pinned in the region of the conduction-band edge at the (100) surfaces of our $p$-PbS samples. An agreement to within 0.1 eV could be achieved for nearly all critical points by shifting the experimental binding energies by 0.3 eV towards lower energies.

The EPM band structure again shows some larger deviations. While the calculated energies for the $\Gamma_8^-$, $\Gamma_6^-$, $L_{45}^{+}/L_6^{+}$, and $\Delta_6$ levels are too large by 0.2–0.3 eV, that of the lowest $X_6^-$ level is too small by 0.2 eV. The agreement between this band-structure calculation and the experimental results would be worse if we would take into account the probable difference between the reference energies.

Thus, we obtain the somewhat surprising result (contrary to some earlier remarks in Ref. 49) that the empirically adjusted band structure exhibits worse agreement with the experimental data than the two first-principle calculations. It is therefore likely that the agreement between calculated and experimental peak energies in the normal emission spectra (cf. Table IV) would be improved upon replacing the EPM valence bands by the APW or OPW valence bands. Yet we should recognize that the observed deviations are rather small in any case, and thus we conclude that the band structure of the $p$-type valence bands of PbS is now know with good accuracy.

Turning to PbSe, we notice more serious deviations between the experimental results and some band-structure calculations even for the bandwidths $\Delta E$ and the energy gap $E_g$. As it has been found in the case of PbS, the APW and OPW calculations predict the experimental results rather well, while the local pseudopotential employed by Kohn *et al.*[11] produces a bandwidth too small by 0.2 eV and an energy gap too large by 0.5 eV. In contrast, the bandwidth obtained from the nonlocal pseudopotential employed by Martinez *et al.*[26] is by far (~ 1.7 eV) too large. These contradictory results should be elucidated in the subsequent detailed comparison of the binding energies of the available three-dimensional critical points.

At point $\Gamma$, we note that the agreement between all four theories and experiment is quite good. At point $X$, the calculated binding energies are all slightly too small by ~ 0.2 eV (except for the nonlocal EPM calculation, which we discard for the moment). Similar results are obtained for the levels with $W_6$, $\Delta_6$, $\Sigma_5$, and $L_{45}^{+}/L_6^{+}$ symmetry, while only the local EPM calculation gives too large binding energies in some cases. The deviations between calculations and experiment could again be minimized by assuming that the Fermi level is pinned close to the conduction-band edge at the (100) surfaces of our PbSe samples.

To summarize, the agreement between the local EPM, OPW, and APW calculations as well as the agreement between these calculations and the experimental results is found to be nearly as good as in the case pf PbS. On the other hand, the nonlocal EPM calculation gives completely different binding energies at point $X$. We emphasize that the observed discrepancies of 0.5–1.3 eV lie far beyond any possible experimental error. The wrong binding energy of the lowest level with $X_6^-$ symmetry is also responsible for the wrong bandwidth at $\vec{k}_{\parallel} = (2\pi/a)(0, 1, 1)$ predicted by the nonlocal EPM band structure. Furthermore, it proves to be impossible to calculate reasonable normal emission spectra on the basis of these valence bands. Especially the peaks marked 2 and 2″ in Fig. 9 would be shifted to considerably higher binding energies. Finally, we note that the total density of valence states calculated by Martinez *et al.*[26] exhibits a pronounced shoulder around 5.5-eV binding energy, which is mainly related to the lowest energy level with $X_6^-$ symmetry. This shoulder is, however, not observed in the XPS[19] and UPS[18] spectra of PbSe (see Fig. 5 of Ref. 26) which should closely resemble the density of valence states. In this respect, the local EPM band-structure calculations also shows better agreement with the experimental results (see Fig. 2 in Ref. 19).

Hence, the calculation that has been fitted to

various experimental data with the highest efforts exhibits the most serious discrepancies. On the other hand, the results of the two first-principles calculations again show surprisingly good agreement with the experimental data.

In PbTe, the bandwidths and the energy gap are reasonably but not accurately reproduced by the calculations. The most important disagreement occurs in the local EPM band structure, here the bandwidth at $\vec{k}_{\parallel} = (2\pi/a)(0, 1, 1)$ is too small by ~ 0.7 eV. The bandwidths predicted by the nonlocal EPM and APW methods appear to be somewhat too large, while the band gap resulting from the APW calculation is too small.

The binding energies of the valence bands at point $\Gamma$ as obtained from the angle-resolved photoemission spectra are larger by 0.2–0.6 eV than those values predicted by the different calculations. At point $X$ also the majority of the calculated binding energies is too small. Nearly all these deviations are again likely to be due to the use of different reference energies for the theoretical and experimental binding energies. The only exception is found in the local EPM band structure which yields by far too small binding energies at point $X$. These deviations of 0.4–1.0 eV have already been noticed in the course of the interpretation of the normal emission spectra, cf. Table III. The wrong binding energy of the lowest energy level with $X_6^-$ symmetry also causes a wrong total bandwidth as mentioned above.

Deviations amounting to as much as 0.5 eV are found at the other critical points. On the whole, the nonlocal EPM band structure seems to agree reasonably with the experimental results. Yet the overall agreement between the different theories and the experimental data is not as good as in PbS and PbSe.

To summarize, we have shown that the valence-band structures of the lead salts (strictly speaking only the $p$-like valence bands) as obtained from angle-resolved photoemission experiments agree quite well with the majority of the band-structure calculations considered here. In particular, the agreement is very good in the case of PbS and PbSe and reasonable for PbTe. The more pronounced deviations in the latter case are perhaps due to the heavy relativistic effects present in the valence bands of PbTe. Furthermore, some of the empirically adjusted band-structure calculations have proved to produce poor results at some critical points. In our opinion, these discrepancies cast some doubt on the usual fitting procedure that solely relies on the adjustment of some characteristic *energy differences* related to the optical properties of the material. In contrast, photoemission measurements can produce reliable *absolute energies*, although it might be difficult to find a suitable common reference energy for both the experimental and calculated binding energies.

### 2. Spin-orbit splittings

Relativistic effects are of importance in the valence bands of all three lead salts. Usually they are divided up into the mass-velocity, the Darwin, and the spin-orbit correction, as may be inferred from the approximate Pauli equation.[21] The first two corrections are invariant under the operations of the single group and therefore do not split levels. They may, however, mix levels of the same single-group symmetry and thereby lead to important rearrangements of their energies.[21] In contrast, the spin-orbit term reduces the orbital degeneracy. Thus degenerate levels may split. The resulting spin-orbit splittings may be observed e.g., in angle-resolved photoemission spectra more readily than the other relativistic effects.

The spin-orbit splittings at the high-symmetry points $\Gamma$, $X$, and $L$ are of special interest. We note that in principle all three points are contained in our experimental $E$-vs-$\vec{k}_{\parallel}$ curves (see Fig. 8), but the identification of the peaks observed at $\vec{k}_{\parallel} = (2\pi/a)(0, \frac{1}{2}, \frac{1}{2})$ has proved to be too difficult to obtain any reliable informations about spin-orbit splittings at point $L$. As outlined above, the angle-resolved photoemission spectra for $\vec{k}_{\parallel} = (2\pi/a)(0, 1, 1)$ closely resemble the one-dimensional density of valence states along the $\Delta$ line. Consequently, these spectra should exhibit spin-orbit-split peaks related to the spin-orbit splittings at $\Gamma$ ($\Gamma_8^-/\Gamma_6^-$) and $X$ ($X_7^-/X_6^-$).

The corresponding HeI-induced spectra are shown in Fig. 16; the electron exit angle $\theta$ decreases according to the decreasing reciprocal-lattice constant $2\pi/a$ in the sequence PbS-PbSe-PbTe. Utilizing NeI photons ($\hbar\omega = 16.85$ eV), it is impossible to fulfill the condition $\vec{k}_{\parallel} = (2\pi/a)(0,1,1)$ because of the lower kinetic energy of the photoelectrons. Spin-orbit splittings are hardly visible in the spectrum of PbS, but are distinct in the second derivative of spectrum shown in the insert. We recall that the expected splittings ($\lesssim 0.25$ eV) are smaller than the resolution (0.3 eV) of the electron energy analyzer. In the spectrum of PbSe, the spin-orbit split peaks are clearly distinguishable. Finally, related peaks are hardly recognizable in the spectrum of PbTe, since the splittings are very large. In particular, the binding energies of the energy levels with $\Gamma_6^-$ and $X_7^-$ symmetry seem to be almost identical.

Numerical values for the spin-orbit splittings

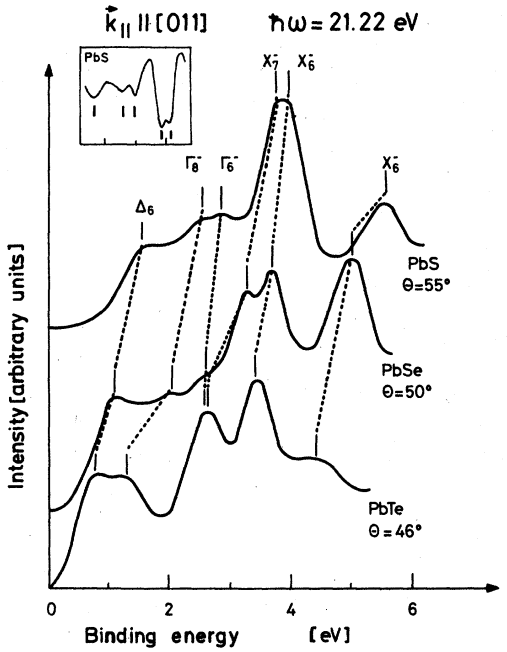


FIG. 16. Angle-resolved photoemission spectra of the lead chalcogenides for $\vec{k}_{\parallel} \simeq (2\pi/a)(0,1,1)$. The second derivative of the spectrum of PbS is shown in the inset.

have not been taken directly from Fig. 16, since the condition $\vec{k}_{\parallel} = (2\pi/a)(0,1,1)$ is rigorously fulfilled only for a special kinetic energy given by $\sqrt{2E} = |\vec{k}_{\parallel}|/\sin\theta$. Quantitative results have therefore rather been obtained from the $E$-vs-$\vec{k}_{\parallel}$ plots shown in Figs. 4–6. Informations regarding the splittings at $X$ are contained in these diagrams also at $\vec{k}_{\parallel} = (2\pi/a)(0,0,1)$ [cf. Fig. 8(a)], while the splittings at $\Gamma$ may also be seen at $\vec{k}_{\parallel} = \vec{0}$. In the latter case, however, the observed peak energies and splittings are likely to be influenced by final-state effects, as outlined in Sec. IV B. Thus, those values obtained at $\vec{k}_{\parallel} = (2\pi/a)(0,1,1)$ and $\vec{k}_{\parallel} = (2\pi/a)(0,0,1)$ are assumed to be most reliable.

In Table V, the experimental results are set next to the calculated spin-orbit splittings as obtained with the four different band-structure calculations already considered in the last section. The EPM calculations employ the scheme developed by Weisz[54] that allows to take into account the spin-orbit interaction within the framework of pseudopotential theory. This scheme contains one or two empirical parameters which are adjusted to give what is believed the "correct" spin-orbit splitting at $\Gamma$. On the other hand, the fully relativistic OPW and APW calculations are both from first principles.

We note that all calculations agree very well with the experimental results as far as the spin-orbit splittings at point $\Gamma$ are concerned. In view of the facts outlined above, this agreement is, however, only significant for the OPW and APW calculations. Moreover, the splitting predicted by the OPW band structure for PbTe is somewhat too small. The observed increase of spin-orbit splittings at $\Gamma$ within the sequence PbS-PbSe-PbTe is related to the increasing spin-orbit splitting of the $p$-valence levels of the chalcogens throughout the sequence.

However, the observed splittings consist of two contributions: (i) one arising from the splitting of the atomic S $3p$, Se $4p$, or Te $5p$ levels (0.10 eV, 0.42 eV, and 0.84 eV,[61] respectively), and (ii) some fraction of the splitting of the atomic Pb $6p$ level, (1.27 eV),[61] which also contributes to the valence bands. We remark that the atomic splittings have to be renormalized according to the different volumes of a free atom and an ion in a solid. Consequently, two important effects have to be taken into account in order to calculate correct spin-orbit splittings: The compression and the hybridization of the outermost $p$ wave func-

TABLE V. Comparison of experimental and theoretical spin-orbit splittings at $\Gamma$ and $X$ in the valence bands of the lead salts.

| | PbS | | PbSe | | PbTe | |
|---|---|---|---|---|---|---|
| | $\Delta_{SO}(\Gamma)$ | $\Delta_{SO}(X)$ | $\Delta_{SO}(\Gamma)$ | $\Delta_{SO}(X)$ | $\Delta_{SO}(\Gamma)$ | $\Delta_{SO}(X)$ |
| Experiment | 0.3 | 0.2 | 0.6 | 0.5 | 1.15 | 0.9 |
| EPM[a,b] | 0.22 | 0.14 | ≃0.55[c] | ≃0.35[c] | 1.09 | ≃0.7[c] |
| EPM[d] | ••• | ••• | 0.55 | ≃0.35[c] | 1.03 | ≃0.55[c] |
| OPW[e] | 0.26 | 0.25 | 0.55 | 0.42 | 1.03 | 0.67 |
| APW[f] | 0.24 | 0.23 | 0.60 | 0.44 | 1.10 | 0.69 |

[a] Reference 11.
[b] Reference 25.
[c] Read from the figure in the corresponding reference.
[d] Reference 26.
[e] Reference 20.
[f] Reference 55.

tions of the atoms. The good agreement between theory and experiment concerning the spin-orbit splittings at $\Gamma$ verify that the relativistic OPW and APW schemes take into account these effects in an appropriate manner.

Finally, we discuss the $\vec{k}$ dependence of the spin-orbit splitting. The decrease of this splitting along the line $\Delta$ may be understood in terms of the following simple argument: At point $\Gamma$ the spin-orbit interaction splits a sixfold degenerate level ($\Gamma_{15}$) into a fourfold ($\Gamma_8^- \rightarrow p_{3/2}$) and a twofold degenerate level ($\Gamma_6^- \rightarrow p_{1/2}$). Assuming a spin-orbit term of the form $\gamma \vec{l} \cdot \vec{s}$ (being valid in the central-field approximation), the resulting splitting is $\frac{3}{2}\gamma$. In contrast, at $X$ a fourfold degenerate level ($X_5'$) is split into two twofold degenerate levels ($X_7^-, X_6^-$), the accompanying splitting is $\gamma$. Thus we obtain the result $\Delta_{so}(X)/\Delta_{so}(\Gamma) = \frac{2}{3}$. Different degrees of hybridization at $\Gamma$ and $X$ are responsible for deviations from the ideal ratio $\frac{2}{3}$.

The experimentally determined decrease of the spin-orbit splitting along the line $\Delta$ amounts to 33%, 17%, and 20% for PbS, PbSe, and PbTe, respectively. Taking into account the experimental uncertainty of ~ 0.1 eV, these results are in fair agreement with the predictions of the OPW and APW calculations. On the other hand, the agreement with both EPM calculations is worse in nearly all cases. Thus, we conclude that the treatment of spin-orbit interaction as employed in the fully relativistic APW[62] and OPW[63] theories is likely to be more adequate than the scheme developed for pseudopotential calculations by Weisz.[54]

## V. CONCLUSIONS

We have presented angle-resolved uv photoemission spectra of the lead chalcogenides PbS, PbSe, and PbTe and discussed their interpretation in terms of the electronic band structures of these compounds. The first attempt to interpret the experimental results was based on the "one-dimensional density-of-states model" which completely neglects momentum conservation in the direction normal to the surface. Thus, experimental peaks are identified with singularities in the one-dimensional density of valence states calculated along $k_\perp$ for fixed $\vec{k}_\parallel$. Although this simple model can account for most of the experimental data, it fails to predict whether a given singularity will show up as a peak. Sometimes even the exact peak energy depends on the photon energy, this also being incompatible with the assumptions of this model. A direct transition model, implying $k_\perp$ conservation, cannot explain the experimental findings either.

The "weighted-indirect-transition model" which contains the above models as limiting cases predicts angle-resolved photoemission spectra that agree quite well with the measured ones. We find that both singularities in the one-dimensional density of states and direct transitions may give rise to peaks, while the relative importance of these two effects is governed by the actual relaxation of $k_\perp$ conservation resulting from the finite photoelectron lifetimes. The good agreement between our calculations which do not rely on the adjustment of empirical parameters and experiments verify that these effects are properly taken into account in the "weighted-indirect-transition model." With the aid of group theory, we show the final-state effects (effects of residual $k_\perp$ conservation) are expected to be most important for normal emission, while the one-dimensional density-of-states model will be more suitable for configurations with lower symmetry, e.g., mirror-plane emission.

Information regarding the valence-band symmetries has been obtained by measuring the dependence of peak intensities on the photon incidence angle. The resulting assignments of peaks to valence bands with different symmetries are fully consistent with the assignments based on the weighted indirect transition model.

Besides these important results concerning the interpretation of angle-resolved photoemission spectra we have presented a detailed comparison of the experimentally obtained valence bands with various band-structure calculations. We have found that from first principles APW and OPW calculations provide good overall pictures of the band structures. Empirically adjusted pseudopotential calculations provide more accurate binding energies for some of the critical points under consideration, while some of the calculated critical points are wrong by as much as ~1 eV. Basically the same holds for measured and calculated spin-orbit splittings: On the one hand, the fully relativistic APW and OPW band structures agree reasonably well with the experimental results, while on the other hand the agreement with the EPM calculations is somewhat worse as far as these calculations provide results that have not explicitly been adjusted.

## ACKNOWLEDGMENTS

We are indebted to Professor S. Rabii for sending us the relativistic crystal potentials for the lead chalcogenides and to Dr. H. Preier for supplying the PbSe samples. Valuable discussions with Dr. A. Liebsch are gratefully acknowledged. Thanks are due to G. Krutina and W. Neu for their assistance.

[1]N. V. Smith, in *Photoemission in Solids* I, edited by M. Cardona and L. Ley (Springer, Heidelberg, 1978), p. 237.
[2]E. O. Kane, Phys. Rev. Lett. 12, 97 (1964).
[3]F.-J. Himpsel and W. Steinmann, Phys. Rev. Lett. 35, 1025 (1975).
[4]W. E. Spicer, Phys. Rev. 112, 114 (1958).
[5]J. B. Pendry and D. J. Titterington, Commun. Phys. 2, 31 (1977).
[6]D. L. Mitchell, E. D. Palik, and J. N. Zemel, in *Physics of Semiconductors*, edited by M. Hulin (Academic, New York, 1964).
[7]A. N. Mariano and K. L. Chopra, Appl. Phys. Lett. 10, 282 (1967).
[8]M. Cardona and D. L. Greenaway, Phys. Rev. 133, A1685 (1964).
[9]D. E. Aspnes and M. Cardona, Phys. Rev. 173, 714 (1968).
[10]T. Nishino, H. Ogawa, and Y. Hamaka, J. Phys. Soc. Jpn. 30, 1113 (1971).
[11]S. E. Kohn, P. Y. Yu, Y. Petroff, Y. R. Shen, Y. Tsang, and M. L. Cohen, Phys. Rev. B 8, 1477 (1973).
[12]G. Martinez, M. Schlüter, and M. L. Cohen, Phys. Rev. B 11, 660 (1975).
[13]U. Büchner, Phys. Status Solidi B 83, 493 (1977).
[14]B. Lahaye, F. Pradal, and C. Gout, J. Phys. (Paris) 4, 137 (1968).
[15]G. Martinez, M. Schlüter, M. L. Cohen, R. Pinchaux, P. Thiry, D. Dagneaux, and Y. Petroff, Solid State Commun. 17, 5 (1975).
[16]M. Cardona, C. M. Penchina, E. E. Koch, and P. Y. Yu, Phys. Status Solidi B 53, 327 (1972).
[17]W. E. Spicer and G. J. Lapeyre, Phys. Rev. 139, A565 (1965).
[18]M. Cardona, D. W. Langer, N. J. Shevchik, and J. Tejeda, Phys. Status Solidi B 58, 127 (1973).
[19]F. R. McFeely, S. Kowalczyk, L. Ley, R. A. Pollack, and D. A. Shirley, Phys. Rev. B 7, 5228 (1973).
[20]F. Herman, R. L. Kortum, I. Ortenburger, and J. P. VanDyke, J. Phys. (Paris) 29, C4 (1968).
[21]L. E. Johnson, J. B. Conklin, Jr., and G. W. Pratt, Jr., Phys. Rev. Lett. 11, 538 (1963); and J. B. Conklin, Jr., L. E. Johnson, and G. E. Pratt, Jr., Phys. Rev. 137, A1282 (1965).
[22]S. Rabii, Phys. Rev. 167, 801 (1968).
[23]H. Overhof and U. Rössler, Phys. Status Solidi B 37, 691 (1970).
[24]P. J. Lin and L. Kleinman, Phys. Rev. 142, 478 (1966).
[25]Y. W. Tung and M. L. Cohen, Phys. Rev. 180, 823 (1969).
[26]G. Martinez, M. Schlüter, and M. L. Cohen, Phys. Rev. B 11, 651 (1975).
[27]T. Grandke, L. Ley, M. Cardona, and H. Preier, Solid State Commun. 24, 187 (1977).
[28]I. Adawi, Phys. Rev. 134, A788 (1964).
[29]G. D. Mahan, Phys. Rev. B 2, 4334 (1970).
[30]W. L. Schaich and N. W. Ashcroft, Solid State Commun. 8, 1959 (1970); and Phys. Rev. B 3, 2452 (1971).
[31]Peter J. Feibelman and D. E. Eastman, Phys. Rev. B 10, 4932 (1974).
[32]J. B. Pendry, *Low-Energy Electron Diffraction* (Academic, London, 1974).
[33]P. O. Nilsson and L. Ilver, Solid State Commun. 17, 667 (1975).
[34]J. Stöhr, G. Apai, P. S. Wehner, F. R. McFeely, R. S. Williams, and D. A. Shirley, Phys. Rev. B 14, 5144 (1976).
[35]H. F. Roloff and H. Neddermeyer, Solid State Commun. 21, 561 (1977).
[36]E. Dietz, H. Becker, and U. Gerhardt, Phys. Rev. Lett. 36, 1397 (1976).
[37]L. Ilver and P. O. Nilsson, Solid State Commun. 18, 677 (1976).
[38]D. R. Lloyd, C. M. Quinn, and N. V. Richardson, J. Phys. C 8, L371 (1975).
[39]J. Stöhr, P. S. Wehner, R. S. Williams, G. Apai, and D. A. Shirley, Phys. Rev. B 17, 587 (1978).
[40]P. Heimann and H. Neddermeyer, J. Phys. F 6, L257 (1976).
[41]S. P. Weeks, Phys. Rev. B 17, 1728 (1978).
[42]R. J. Smith, J. Anderson, J. Hermanson, and G. J. Lapeyre, Solid State Commun. 19, 975 (1976).
[43]G. J. Lapeyre, R. J. Smith, and J. Anderson, J. Vac. Sci. Technol. 14, 384 (1977).
[44]N. E. Christensen and B. Feuerbacher, Phys. Rev. B 10, 2349 (1974).
[45]P. Heimann, H. Neddermeyer, and H. F. Roloff, Phys. Rev. Lett. 37, 775 (1976).
[46]D. Liebowitz, J. Muratore, Y. H. Kao, and N. J. Shevchik, Solid State Commun. 22, 759 (1977).
[47]B. Feuerbacher and N. E. Christensen, Phys. Rev. B 10, 2373 (1974).
[48]C. Noguera, D. Spanjaard, and D. W. Jepsen, Proceedings of the Fifth International Conference on Vacuum Ultraviolet Radiation Physics, edited by M. C. Castex, M. Pouey, and N. Pouey, Meudon, 1977 (unpublished), Vol. II, p. 153.
[49]Thomas Grandke, Lothar Ley, and Manuel Cardona, Phys. Rev. Lett. 38, 1033 (1977); and T. Grandke, L. Ley, and M. Cardona, Solid State Commun. 23, 897 (1977).
[50]H. Maier, D. R. Daniel, and H. Preier, J. Cryst. Growth 35, 121 (1976).
[51]A. L. Hagström, dissertation (Linköping, Sweden, 1977) (unpublished).
[52]M. Green and M. J. Lee, J. Phys. Chem. Solids 27, 797 (1966).
[53]Roy F. Willis, Phys. Rev. B 17, 909 (1978).
[54]G. Weisz, Phys. Rev. 149, 504 (1966).
[55]S. Rabii and R. H. Lasseter, Phys. Rev. Lett. 33, 703 (1974); and T. Grandke and S. Rabii (unpublished).
[56]J. C. Slater and G. F. Koster, Phys. Rev. 94, 1498 (1954).
[57]D. J. Chadi, Phys. Rev. B 16, 790 (1977).
[58]J. Hermanson, Solid State Commun. 22, 9 (1977).
[59]D. Liebowitz, M. Sagurton, J. Colbert, and N. J. Shevchik, Phys. Rev. Lett. 39, 1625 (1977).
[60]M. Scheffler, K. Kambe, and F. Forstmann, Solid State Commun. 23, 789 (1977).
[61]F. Herman and S. Skillman, *Atomic Structure Calculations* (Prentice-Hall, Englewood Cliffs, N.J., 1963).
[62]T. L. Loucks, Phys. Rev. 139, A1333 (1965).
[63]P. Soven, Phys. Rev. 137, A1706 (1965).